Maximilian Wetzlinger, BSc

Efficiency-optimized control strategy for a cooling system

Master's Thesis

to achieve the university degree of
Diplom-Ingenieur

Master's degree programme: Electrical engineering

submitted to
Graz University of Technology

Supervisor
Univ.-Prof. Dipl-Ing. Dr.techn. Martin Horn

Institute of Automation and Control

Graz, June 2016

This work was accomplished at the VIRTUAL VEHICLE Research Center in Graz, Austria. The author would like to acknowledge the financial support of the COMET K2 - Competence Centers for Excellent Technologies Programme of the Austrian Federal Ministry for Transport, Innovation and Technology (bmvit), the Austrian Federal Ministry of Science, Research and Economy (bmwfw), the Austrian Research Promotion Agency (FFG), the Province of Styria and the Styrian Business Promotion Agency (SFG).

He would furthermore like to express his thanks to Univ.-Prof. Dipl-Ing. Dr.techn. Martin Horn, Dipl.-Ing. Armin Traussnig and Dipl-Ing. Dr.techn. Michael Stolz.

Statutory Declaration

I declare that I have authored this thesis independently, that I have not used other than the declared sources/resources, and that I have explicitly marked all material which has been quoted either literally or by content from the used sources.

Graz, _____ _____

Date Signature

Eidesstattliche Erklärung[1]

Ich erkläre an Eides statt, dass ich die vorliegende Arbeit selbstständig verfasst, andere als die angegebenen Quellen/Hilfsmittel nicht benutzt, und die den benutzten Quellen wörtlich und inhaltlich entnommenen Stellen als solche kenntlich gemacht habe.

Graz, am _____ _____

Datum Unterschrift

[1] Beschluss der Curricula-Kommission für Bachelor-, Master- und Diplomstudien vom 10.11.2008; Genehmigung des Senates am 1.12.2008

Abstract

In common vehicles the temperature control of the engine or e-motor cooling system is mostly done by a simple bang-bang control of the cooling fan speed and pump speed, or even only with a bypass and a wax thermostat valve. In this work a more sophisticated control strategy was implemented. Therefore, a test bench was set up at the Virtual Vehicle Research and Test Center. It consists of a conditioning unit with coolant pump and heating element, a windtunnel and a passenger car heat exchanger. For simulation purposes a Simulink model of the test bench was implemented. Therefore, the cooling circuit's and the heat exchanger's thermal behaviour was measured. The parameters of the simulated heat exchanger were fitted in a least squares sense to match its real life pendant.
The control development required dividing the non-linear mathematical model of the cooling circuit into a linear and a non-linear part. For the linear part a Constrained Model Predictive Control (CMPC) was implemented which provides a reference cooling capacity for the heat exchanger as result. Additionally, a linear interpolation of two different CMPC was done as the coolant mass flow changes the dynamic of the linear system. The reference cooling capacity is then fed to a heat exchanger inversion where, depending on the current vehicle speed, a fitting fan speed is calculated.
As only two temperatures in the cooling circuit were measured, a PI observer was implemented. The observer estimates all state variables of the system plus the heating power of the conditioning unit, which was treated as a disturbance variable. The whole control concept was tested at the test bench as well as in the simulation and compared to each other. Also the difference between a Bang-Bang control system and the CMPC was simulated and discussed.

Contents

Abstract iv

1 Introduction 1

2 Test bench setup 4

3 Thermal modeling 12
- 3.1 Heat exchanger modelling . . . 15
  - 3.1.1 Convective heat transfer rates . . . 16
  - 3.1.2 Calculation of the cooling capacity . . . 19
- 3.2 Complete Simulation model . . . 20

4 Heat exchanger model - optimization 23

5 Control strategy 27
- 5.1 Linearization . . . 27
  - 5.1.1 Linear time-invariant state space model . . . 27
- 5.2 Control design . . . 30
  - 5.2.1 Model predictive control . . . 32
  - 5.2.2 Proportional-integral (PI) observer . . . 44
  - 5.2.3 Heat exchanger inversion . . . 50
  - 5.2.4 MPC Interpolation . . . 51

6 Results 53
- 6.1 Comparison of test bench setup to simulation . . . 53
- 6.2 Comparison bang-bang control to MPC . . . 56
- 6.3 Outlook and Limitations . . . 58

Bibliography 59

1 Introduction

Over the last decades an enormous effort has been made to reduce fuel consumption and CO_2 emission of passenger cars and commercial vehicles. The greatest part of research and development focused on enhancing the combustion engine, gas exchange and engine control systems. While the potential to reduce emissions decreased, the costs of development rose. To reduce the emission of greenhouse gases further, new technologies had to be found. One of these relatively young research areas is *vehicle thermal management*. It deals with the heat/energy flow in the vehicle. By using enhanced control strategies power consumption for several auxiliary components can be saved, leading to less fuel consumption in the end [12].
The priniciple of an engine cooling system has not changed dramatically since nearly the invention of the automobile. As can be seen in Figure 1.1, the main components of cooling systems are a thermostat, a heat exchanger and a belt-driven pump [2]. The engine can be regarded as a heat source. If not only the pump but also the fan engine attached to the heat exchanger is belt-driven, there is just one way to control the engine's operating temperature, which is the thermostat. These thermostats that are used in cars are also known as "engine-coolant control valves". Since the cooling system has to be designed in a way that it can handle the maximum heat load by even little vehicle speed, for example stop-and-go traffic or climbing hills, the radiator is oversized under normal conditions. Without the thermostat, the cooling system would always operate at full capacity, which then would lead to engine temperatures below the optimum.
The thermostat senses the coolant temperature and controls the ratio between the coolant flow through the radiator and the bypass. By doing so, it is possible to keep the engine temperature at a range of tolerance around the setpoint temperature. If the coolant temperature is too low, the

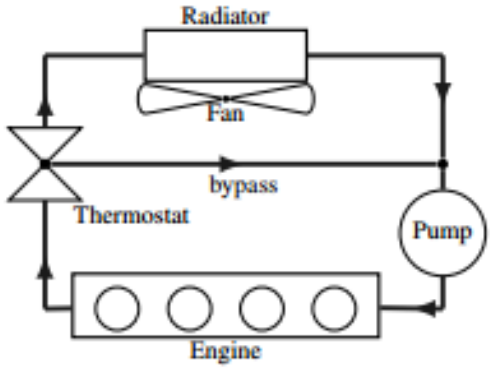

Figure 1.1: Typical structure of an engine cooling system [2]

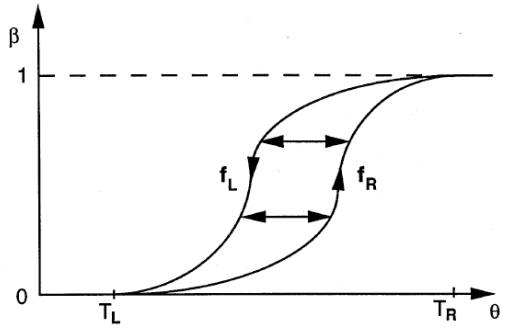

Figure 1.2: Opening and closing behaviour of a thermostat [18]

thermostat closes the loop over the radiator to avoid cooling. Otherwise, if the temperature is too high, the bypass-loop is completely closed and the cooling system works at its full capacity. Although thermostats are based on a very simple concept, the dynamic behaviour of the wax melting and solidification process is much more complicated. In general they tend to have a hysteresis in their opening/closing operation, as can be seen in Figure 1.2. The graph describes the opening and closing of a thermostat as a function of the coolant's temperature where $\beta = 1$ means that the whole coolant flow passes the radiator [18]. As a result of this hysteresis the engine temperature tends to overshoot or oscillate around the setpoint of the controlled system.

1 Introduction

By introducing electrical driven pumps and fans, more degrees of freedom are available to the control unit. Various contributions, dealing with energy saving and electrification of the motor cooling system, have been published in the recent years. Nevertheless, in today's vehicles, if there is an electrically driven fan at all, the control strategy is just a Bang-Bang-control, which leads again to an oscillating behaviour. As part of this thesis a test bench of an engine cooling system has been built and a model predictive control with the radiator's fan speed as correcting variable was developed. By implementing this more sophisticated control concept, numerous enhancements can be achieved. The main point is to get the engine's coolant temperature to its setpoint without overshoot. If this can be guarenteed, the desired temperature may be increased, which leads again to several improvements. Firstly, as a result of the higher engine temperature, the friction in the engine decreases. Secondly, the gap between ambient air temperature and coolant temperature will be higher so that the energy consumption of the fan decreases. All this together leads to lower fuel consumption in the end.

2 Test bench setup

For the practical and experimental part of the thesis, a test bench was built at the Virtual Vehicle Resarch and Test Center. The radiator was dismounted from a BMW X3, 3.0 HSDI. The parameters of the heat exchanger were already measured as part of a previous thesis at the Virtual Vehicle [11]. As heat source and also as coolant pump a conditioning unit was used. The heat source can be modulated from $0kW$ up to $72kW$ in $0.72kW$ steps. The adjustable coolant pump produces a mass flow between approximately $3\frac{kg}{min}$ as far as $120\frac{kg}{min}$. Additionally, the heat exchanger was attached to a wind tunnel to test it under different air mass flows. In Figure 2.1 the complete test bench setup is illustrated.

Due to the reason that both flow and return pipe are almost 10 meters long and uninsulated, the convective heat loss to the ambient air can not be neglected. In table 2.3 the heat transfer rate of the conditioning unit and the cooling capacity of the heat exchanger are shown. It can be observed that if the average coolant temperature rises, also the difference between the heating power $\dot{Q}_{HS}$ and the cooling capacity $\dot{Q}_{HX}$ increases. Some fundamental dimensions of the heat exchanger are summerized in table 2.1.

In figure 2.2 the experimental setup of the test bench can be seen. Also all measured variables are displayed, whereat $T_{Air,in}$ is the mean value of 4 Pt-100 temperature sensors and $T_{Air,out}$ is the mean value of 6 thermo wires. The Pt-100 sensors were placed at the side surfaces of the wind tunnel's inside and the thermo wires were mounted at the radiator's air outlet as a 2 times 3 array to reduce the error of measurement. With the measured values of the two volumetric instruments and the corresponding relative density, the mass flow of air and coolant can be determined.

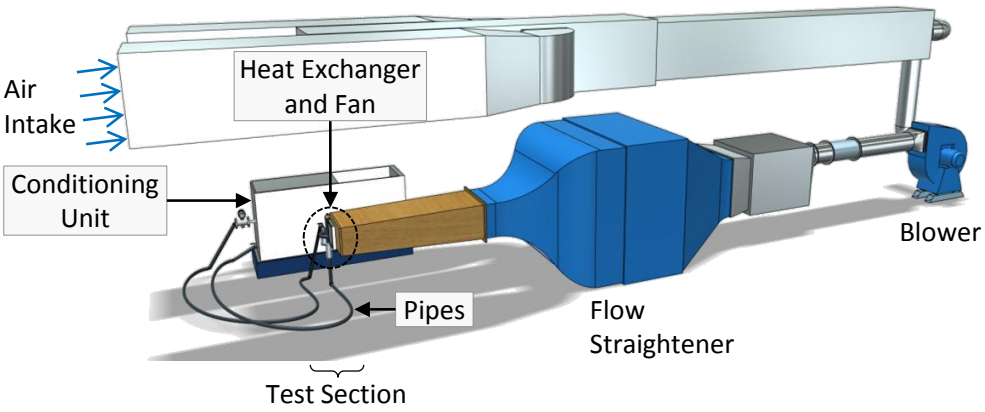

Figure 2.1: Testbed at the Virtual Vehicle Resarch and Test Center [14]

HX height in m	0.51
HX width in m	0.59
HX depth in m	0.03
Number of Passes	1
Number of Tubes per Pass	52
HX mass in kg	3
Fin Thickness in m	0.0004
Fin Pitch in m	0.001
Tube Thickness in m	0.002
Louver Angle in degrees	27
Louver Pitch in m	0.001
Coolant Volume in l	3
Numbers of Cells per Pass	2
Wall Thickness in m	0.0035
Wall conductivity	250

Table 2.1: Main parameters of the heat exchanger

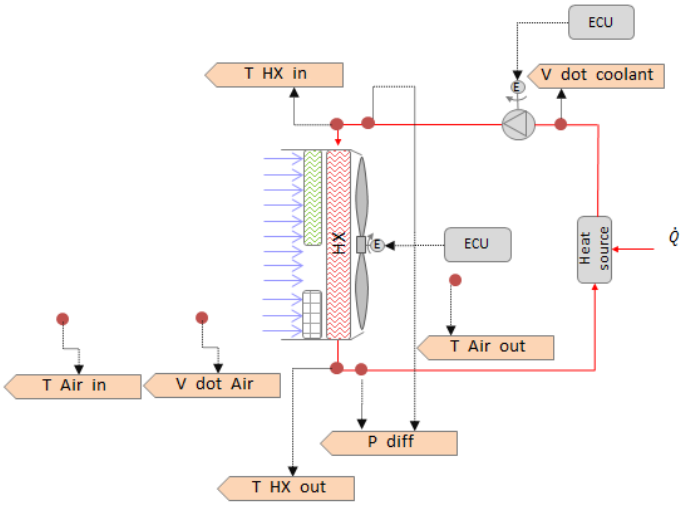

Figure 2.2: Measuring setup of the cooling circuit

To identify the thermal behaviour of the cooling circuit the following measurements as in table 2.3, were carried out. The purpose of measurement No. 1 was to determine the thermal inertia of the system (figure 2.3). The other experiments were done to find steady states (2.4). In these states the heating power of the heat source and the cooling capacity of the heat exchanger, together with the convective heat loss in the pipes, are in balance, i.e.

$$\text{Heating power} = \text{Heat exchanger cooling} + \text{Pipe heat loss}. \tag{2.1}$$

To find these steady states, the coolant temperature was observed. For both constant coolant and air mass flow, it can be stated that the system is in a steady state, if the coolant temperature in the circuit does not change over time. With the knowledge of these steady states the characteristics of the radiator can be determined. To make sure that the temperature sensors work properly, the cooling capacity of the heat exchanger was calculated in two ways.

Variable	Description
$\dot{Q}_{HS}$	Heating power of the conditioning unit
$\dot{m}_{co}$	Coolant mass flow
$\dot{m}_{air}$	Air mass flow
$T_{air,i}$	Air inlet temperature
$T_{air,o}$	Air outlet temperature
$T_{HX,i}$	Coolant temperature at heat exchanger inlet
$T_{HX,o}$	Coolant temperature at heat exchanger outlet
$\dot{Q}_{HX}$	Cooling capacity of the heat exchanger

Table 2.2: Description of the measured variables

No.	$\dot{Q}_{HS}$	$\dot{m}_{co}$	$\dot{m}_{air}$	$T_{air,i}$	$T_{air,o}$	$T_{co,i}$	$T_{co,o}$	$\dot{Q}_{HX}$
	kW	$\frac{kg}{s}$	$\frac{kg}{s}$	$°C$	$°C$	$°C$	$°C$	kW
1	50.4	2	0	–	–	–	–	–
2	10.8	0.1	0.6	24.4	–	50	36	6
3	25.2	0.6	0.3	12	78.9	96.3	88.3	17.2
4	25.2	0.6	0.5	11.6	68.6	87.4	78.9	18.1
5	25.2	0.6	1	12.7	49.7	66.1	57.4	19.6
6	25.2	0.6	1.2	9.4	30.8	49.7	39.8	20.7
7	25.2	1.2	0.4	8.8	27.7	46.8	36.8	20.8
8	35.3	1.2	0.6	12.1	78.2	94.4	88.2	26.9
9	35.3	1.2	1	11.4	59	76.5	69.8	28.8
10	35.3	1.2	1.2	9.5	40.3	59.5	52.5	29.8
11	35.3	1.8	0.6	9.4	35.3	54.9	47.8	29.9
12	50.4	1.8	1	12.3	74.84	92.3	86.2	38.9
13	50.4	1.8	1.2	11.9	52.8	73.5	66.8	42.3
14	50.4	1.8	1.5	11.8	47	69	62.3	42.5
15	50.4	1.8	1.8	12.2	40	63.5	56.7	42.9
16	50.4	0.1	0.6	12.9	35.9	60.6	53.8	42.6

Table 2.3: List of measurement

The coolant and the air side of the heat exchanger can be seen as two open systems which are connected over the heat transfer rate $\dot{Q}_{HX}$. For vehicle velocities less then Mach 0.3 the air can be seen as incompressible and therefore can be treated the same as the coolant fluid. If the cooling system is in a steady state which means that the coolant temperature does not change over time, the two open systems can be described with equations (2.2) and (2.3) as follows:

$$0 = \dot{Q}_{HX} + \dot{m}_{air} \left[\left(\overline{c_p}_{air} T_{air} \right)_i - \left(\overline{c_p}_{air} T_{air} \right)_o \right], \tag{2.2}$$

$$0 = -\dot{Q}_{HX} + \dot{m}_{co} \left[\left(\overline{c_p}_{co} T_{HX} \right)_i - \left(\overline{c_p}_{co} T_{HX} \right)_o \right], \tag{2.3}$$

where $\overline{c_p}$ is the integral specific heat capacity of the air, respectively the coolant, as defined in equation (3.12).
The heat transfer rate $\dot{Q}_{HX}$ can be interpreted as the cooling capacity of the heat exchanger. By measuring both mass flows as well as inlet and outlet temperature of air and coolant, the cooling capacity can be balanced in two separate ways.

In figure 2.3 the heating process (measurement No. 1) of the cooling circuit is shown. In comparison to figure 2.4 there is no air mass flow which results in an integral behaviour of the coolant temperature. In comparison to the heating power $\dot{Q}_{HS}$ and the coolant mass flow, the pipe's convective heat loss is small and shows small impact on the coolant temperature. Figure 2.5 shows the comparison of the two calculated cooling capacities for measurement number 5. Compared to the heating power in table 2.3, the cooling capacity is about $5kW$ smaller, which can be explained by the already mentioned convective heat loss in the pipes.

The excitation of the fan drive is done by a $12V$ pulse width modulated (PWM) signal, with a frequency of about $120Hz$. The PWM signal is created by an *Arduino* board, which is linked to a notebook with *Matlab*. Also, all sensor data required for the control strategy later on, is provided to *Matlab* via a *National Instrument USB-6009 Data Acquisition* device and the *Matlab Data Acquisition Toolbox*. As both *Matlab* and the *Data Acquisition Toolbox* are operating in a non-real time environment, there is a possibility

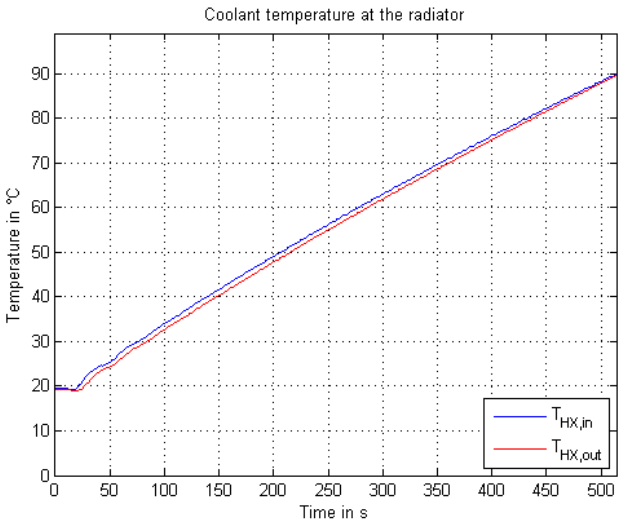

Figure 2.3: Coolant temperature measurement number 1

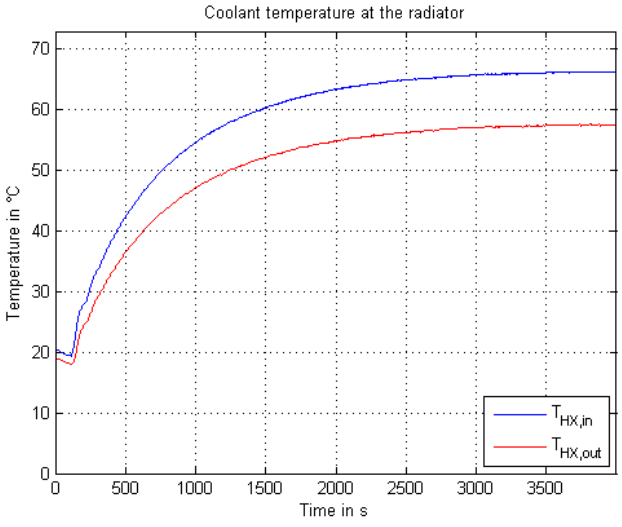

Figure 2.4: Coolant temperature measurement number 5

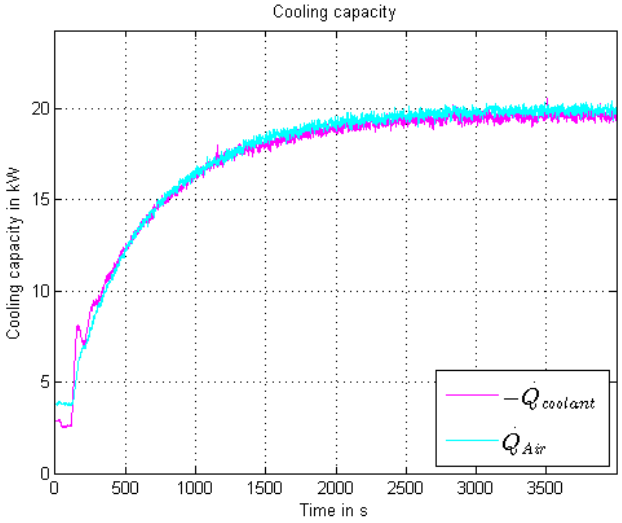

Figure 2.5: Cooling capacity measurement number 5

of jitter in the closed loop control. However, due to the reason that the *DAQ Toolbox* and the PI observer work with a 20 times higher sampling rate than the Model Predictive Control, it is assumed that the impact of jitter is neglectable.
In figure 2.6 the characteristic curve of the cooling fan and in figure 2.7 the air mass flow as a function of the vehicle's velocity and the fan rotational speed are shown. As it can be seen, for a large duty range the air mass flow, produced by the cooling fan, is linear related to the duty-factor of the PWM signal. A duty-factor below 9% and above 94% is reserved for trouble shooting and can not be used to generate an air mass flow. This especially leads to problems with very low required air mass flows, as they can not be generated. On that account there is some sort of bang-bang-principle at the beginning of the cooling process, which can be seen in figure 5.7.

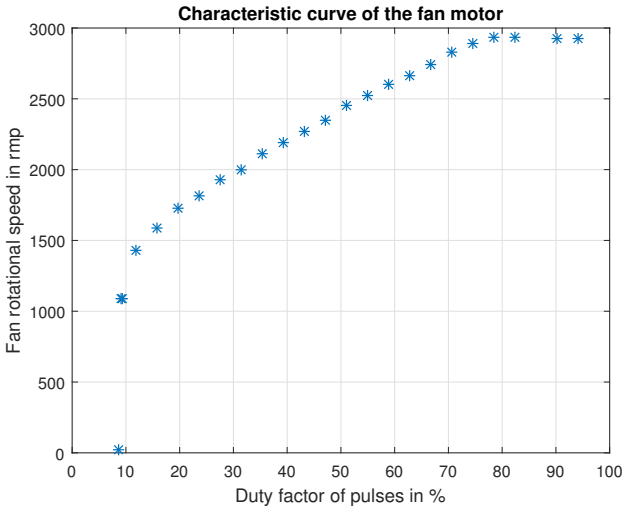

Figure 2.6: Fan rotational speed as function of the duty factor

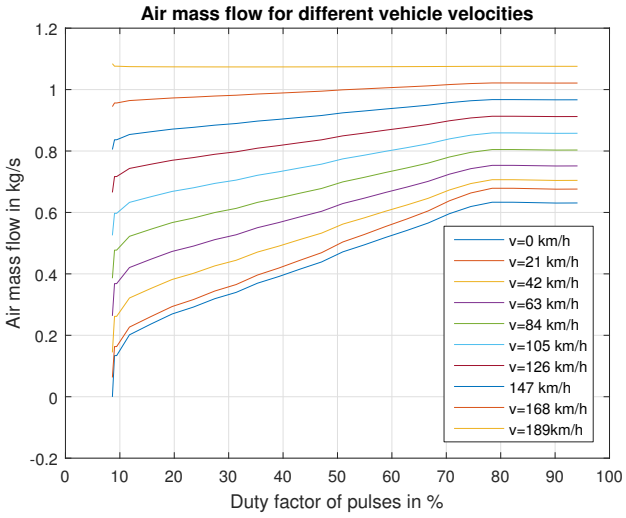

Figure 2.7: Air mass flow as function of vehicle velocity and fan speed

3 Thermal modeling

The first law of thermodynamics

$$\Delta E = Q + W \tag{3.1}$$

states, that the change of the total energy E of a closed system is the sum of transferred heat Q and transferred work W into the system. Furthermore, a system's energy can be separated into potential energy E_{pot}, kinetic energy E_{kin} and internal energy U.

$$\Delta E = \Delta \left(E_{pot} + E_{kin} + U \right) \tag{3.2}$$

The enthalpy H is defined as the sum of the internal energy U and the product of pressure p and volume V.

$$H = U + pV \tag{3.3}$$

By assuming that no work W is done in the cooling circuit and by neglecting the change of kinetic and potential energy, equations (3.1) can be written for a control volume as:

$$\Delta H = Q + \Delta \left(pV \right). \tag{3.4}$$

However, open systems do have a mass flow $\dot{m}$ going into or out of a control volume. Dealing with such a system, the enthalpy flow

$$\dot{H} = \dot{m}h \tag{3.5}$$

must be taken into consideration, as it changes the energy in a control volume.

As the cooling circuit will be described as several open control volumes, it is assumed that there are constant volumes with no mass accumulation. Also the change of internal energy due to pressure changes is neglected.

Under these assumptions the first law of thermodynamics for open systems for an infinitesimal time step can be written as [16]

$$\frac{dH}{dt} = \left(\dot{Q} + \dot{H}\right)_{in-out}, \tag{3.6}$$

where enthalpy flows $\dot{H}$ and heat transfer rates $\dot{Q}$ into the system are counted positive and out of the system negative. The left side of equation (3.6) can be written as [16]

$$\frac{dH}{dt} = \frac{d\left(mh\right)}{dt} = V\rho\frac{dh}{dt} + h\frac{d\left(V\rho\right)}{dt}. \tag{3.7}$$

Due to the assumption that it is only dealt with open systems with constant volume and no mass accumulation, the equation simplifies to:

$$\frac{dH}{dt} = \frac{d\left(mh\right)}{dt} = m\frac{dh}{dt}. \tag{3.8}$$

For systems with constant pressure the specific enthalpy h of a system with the temperature T_1 can be calculated with the integral equation

$$h = \int_0^{T_1} c_p dT. \tag{3.9}$$

By defining the specific heat capacity c_p as a second degree polynomial depending on the substance's temperature

$$c_p = a + bT + cT^2, \tag{3.10}$$

equation (3.9) can be solved to

$$h = T_1 \left(a + \frac{bT_1}{2} + \frac{cT_1^2}{3} \right). \tag{3.11}$$

By introducing a integral specific heat capacity

$$\overline{c_p} = a + \frac{bT}{2} + \frac{cT^2}{3}, \tag{3.12}$$

equation (3.9) can be simplified to

$$h = \overline{c_p} T_1. \tag{3.13}$$

With this simplification equation (3.8) can be written as

$$\frac{dH}{dt} = m\overline{c_p}\frac{dT}{dt} \tag{3.14}$$

By combining equations (3.5), (3.6), (3.13) and (3.14) the first law of thermodynamics can be written as [15]

$$m\overline{c_p}\left(T_{out}\right)\frac{dT_{out}}{dt} = \dot{Q}_{in} - \dot{Q}_{out} + \dot{m}\left[\left(\overline{c_p}T\right)_{in} - \left(\overline{c_p}T\right)_{out}\right] \tag{3.15}$$

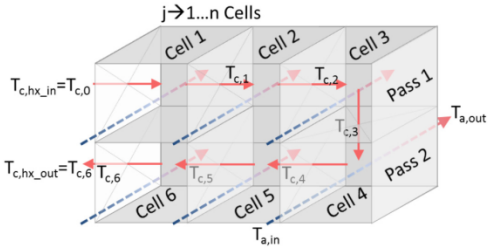

Figure 3.1: Discretized heat exchanger model [15]

3.1 Heat exchanger modelling

The heat exchanger on the coolant side can be described with equation (3.15) as follows:

$$m\overline{c_p}_{co,o}\frac{dT_{HX,o}}{dt} = \dot{Q}_{HX} + \dot{m}_{co}\left(\overline{c_p}_{co,i}T_{HX,i} - \overline{c_p}_{co,o}T_{Hx,o}\right). \tag{3.16}$$

To improve the accuracy of the simulation model, the heat exchanger has been discretized into cells along the axis of the coolant flow [15]. For each cell, equation (3.16) is used where the temperature of the ingoing coolant is either the coolant temperature at the heat exchanger entry or the temperature of the outgoing coolant of the previous cell. The total cooling capacity of the heat exchanger is the sum of the cooling capacities of all cells. In figure 3.1 a heat exchanger model with six cells is shown. While the coolant temperature changes from cell to cell, it is assumed that the ingoing air temperature is the same for all cells. For simplification of the following equations it is assumed that the heat exchanger model only consists of one cell.

To calculate the cooling capacity $\dot{Q}_{HX}$ of the heat exchanger, the thermal resistance concept is being used. The concept draws comparisons between a thermal and an electrical network where a temperature difference can be seen as voltage and a heat transfer rate as current.

$$\dot{Q}_{HX} = \frac{\Delta T}{R_{HX}} \tag{3.17}$$

In the case of a liquid\air heat exchanger, the thermal resistance can be modeled as a serial connection of three thermal resistances

$$R_{HX} = R_{co} + R_{wall} + R_{air}, \tag{3.18}$$

where R_{co} represents the convection resistance from the coolant to the heat exchanger's wall, R_{wall} is the convection resistance of the heat exchanger material and R_{air} stands for the resistance from the heat exchanger to the bypassing air. While R_{wall} can be seen as a constant factor, the two other thermal resistances depend on temperature and mass flow of the coolant and air respectively. Both can be written as the reciprocal value of the product of heat transfer area A_{ht} and convective heat transfer coefficient α:

$$R_{co} = \frac{1}{\alpha_{co} A_{ht,co}}, \tag{3.19}$$

$$R_{air} = \frac{1}{\alpha_{air} A_{ht,air}} \tag{3.20}$$

3.1.1 Convective heat transfer rates

As mentioned before, the convective heat transfer coefficient depends on temperature and mass flow (velocity) of the fluid or gas, and is therefore not easy to determine. A common approach is the calculation of the dimensionless Nusselt number Nu. This coefficient can be seen as the ratio of convective heat transfer of a flowing fluid to conductive heat transfer of a motionless fluid which gives

$$Nu = \frac{\dot{q}_{conv}}{\dot{q}_{cond}} = \frac{\alpha \Delta T}{\frac{k \Delta T}{d_{hyd}}} = \frac{\alpha d_{hyd}}{k}, \tag{3.21}$$

where k is the thermal conductivity and d_{hyd} is the characteristic length. So if the Nusselt number is known, the convective heat transfer coefficient can be calculated by rearranging equation (3.21).

Nusselt number of the coolant

One way to determine the Nusselt number of the coolant is equation (3.22) [3], where the Nusselt number is a function of the Reynolds number and the Prandtl number. The coefficients a,b and c are later determined by the least squares method.

$$Nu_{co} = aRe_{co}^{b}Pr_{co}^{c} \tag{3.22}$$

The Reynolds number Re represents the ratio of inertia forces to viscous forces in the fluid and depends mainly on geometry, free stream velocity, temperature and fluid type and is expressed as

$$Re_{co} = \frac{\text{inertia forces}}{\text{viscous forces}} = \frac{v_{co}d_{hyd,co}}{\nu_{co}} = \frac{\frac{\dot{m}_{co}}{\rho_{co}A_{flow,co}z}d_{hyd,co}}{\nu_{co}} \tag{3.23}$$

where ν_{co} is the kinematic viscosity of the fluid and v_{co} is the fluid velocity. The fluid velocity can be calculated by dividing the coolant mass flow by the product of the tube free flow area $A_{flow,co}$, the number of tubes per pass in the heat exchanger z and the coolant density ρ_{co}.

The Prandtl number Pr is defined as the ratio of kinematic viscosity ν_{co} to thermal diffusivity $a_{th,co}$

$$Pr_{co} = \frac{\nu_{co}}{a_{th,co}} = \frac{\nu_{co}}{\frac{k_{co}}{c_{p,co}\rho_{co}}} = \frac{\nu_{co}c_{p,co}\rho_{co}}{k_{co}}, \tag{3.24}$$

where ρ_{co} is the coolant's density and k_{co} is the thermal conductivity. The four parameters

- thermal conductivity k_{co}

- specific heat capacity $c_{p,co}$
- density ρ_{co}
- and kinematic viscosity ν_{co}

are all temperature-dependent and can be determined by simple look-up tables with the coolant temperature as input.

Nusselt number of the streaming air

As it can be assumed that the vehicles move with under $100\frac{m}{s}$, the air can be treated as an incompressible fluid. To calculate the Nusselt number of the air, the modified Reynolds analogy [3] is being used.

$$Nu_{air} = jRe_{air}Pr_{air}^{\frac{1}{3}} \tag{3.25}$$

The Reynolds number of the streaming air Re_{air} can be determined the same way as for the coolant. The air free flow area is defined as

$$A_{flow,air} = \left(hx_{height} - zt_t\right) hx_{width} - \frac{hx_{width}}{f_p}\left(hx_{height} - zt_t\right) f_t hx_{width} \tag{3.26}$$

and as characteristic length the louver pitch l_p is used. The Prandtl number Pr_{air} is determined directly from a look-up table with the air temperature as input. The factor j is called Colburne - Factor and is defined by Chang and Wang [4] for louver fin geometry as follows:

$$j = Re_{air}^{-0.49}\left(\frac{l_a}{90}\right)^{0.27}\left(\frac{f_p}{l_p}\right)^{-0.14}\left(\frac{f_h}{l_p}\right)^{-0.29}\left(\frac{f_d}{l_p}\right)^{-0.23}\left(\frac{l_l}{l_p}\right)^{0.68}\left(\frac{f_h+t_t}{l_p}\right)^{-0.28}\left(\frac{f_t}{l_p}\right)^{-0.05} \tag{3.27}$$

- $l_a \ldots$ louver angle
- $f_p \ldots$ fin pitch
- $l_p \ldots$ louver pitch
- $f_h \ldots$ fin height
- $f_d \ldots$ fin depth
- $l_l \ldots$ louver length
- $t_t \ldots$ tube thickness

- $f_t \ldots$ fin thickness
- hx_{width} heat exchanger width
- hx_{height} heat exchanger height
- z number of tubes per pass

To determine the convective heat transfer coefficient for the air side, a factor η for fin efficiency is added to equation (3.21):

$$\alpha_{air} = \eta \frac{Nu_{air} k_{air}}{d_{hyd,air}} \tag{3.28}$$

3.1.2 Calculation of the cooling capacity

To calculate the temperature difference ΔT in equation (3.17), the logarithmic mean temperature difference is being used [16]

$$\Delta T = \frac{\Delta T_1 - \Delta T_2}{\ln\left(\frac{\Delta T_1}{\Delta T_2}\right)}, \tag{3.29}$$

where ΔT_1 represents the temperature difference of coolant and air at the air intake and ΔT_2 the temperature difference at the air exit. It is assumed that the temperature of the coolant only changes in the direction of the coolant flow and not in the direction of the air flow. Therefore, the coolant temperatue at the air entry and at air exit is the same. As the heat exchanger is being discretized in the direction of the coolant flow, the mean temperature of the coolant in each cell is defined as the coolant temperature at the exit of the same cell. On that account the two temperature differences can be written as

$$\Delta T_1 = T_{air,in} - T_{co,out}, \tag{3.30}$$

$$\Delta T_2 = T_{air,out} - T_{co,out}. \tag{3.31}$$

To calculate the air outlet temperature $T_{air,out}$ the analytical quasi static solution for the logarithmic mean air temperature distribution [15] is being used:

$$T_{air,o} = T_{air,i} + \left(1 - exp\left(-\frac{\alpha_{air} A_{ht,air}}{\dot{m}_{air} c_{p,air}}\right)\right)(T_w - T_{air,i}), \tag{3.32}$$

with the temperature of the heat exchanger wall

$$T_w = T_{co,out} + R_{co}\dot{Q}_{HX}. \tag{3.33}$$

3.2 Complete Simulation model

The cooling circuit of the test bench is described by four differential equations

$$m_{pipe1}\bar{c}_{p,HS,i}\frac{dT_{HS,i}}{dt} = \dot{m}_{co}\left(\bar{c}_{p,HX,o}T_{HX,o} - \bar{c}_{p,HS,i}T_{HS,i}\right) + \dot{Q}_{pipe1} \tag{3.34}$$

$$m_{HS}\bar{c}_{p,HS,o}\frac{dT_{HS,o}}{dt} = \dot{m}_{co}\left(\bar{c}_{p,HS,i}T_{HS,i} - \bar{c}_{p,HS,o}T_{HS,o}\right) + \dot{Q}_{HS} \tag{3.35}$$

$$m_{pipe2}\bar{c}_{p,HX,i}\frac{dT_{HX,i}}{dt} = \dot{m}_{co}\left(\bar{c}_{p,HS,o}T_{HS,o} - \bar{c}_{p,HX,i}T_{HX,i}\right) + \dot{Q}_{pipe2} \tag{3.36}$$

$$m_{HX}\bar{c}_{p,HX,o}\frac{dT_{HX,o}}{dt} = \dot{m}_{co}\left(\bar{c}_{p,HS,i}T_{HS,i} - \bar{c}_{p,HX,o}T_{HX,o}\right) + \dot{Q}_{HX} \tag{3.37}$$

$$\bar{c}_{p,i} = f\left(T_i\right) \tag{3.38}$$

and the corresponding equations, which describe the heat transfer rates:

$$\dot{Q}_{pipe1} = K\left(T_{air,i} - \frac{T_{HX,o} + T_{HS,i}}{2}\right) \tag{3.39}$$

$$\dot{Q}_{pipe2} = K\left(T_{air,i} - \frac{T_{HS,o} + T_{HX,i}}{2}\right) \tag{3.40}$$

$$\dot{Q}_{HX} = \frac{\Delta T}{R_{HX}} \tag{3.41}$$

$$R_{HX} = R_{co} + R_{wall} + R_{air} \tag{3.42}$$

$$R_{co} = \frac{1}{\alpha_{co} A_{co}} \tag{3.43}$$

$$R_{air} = \frac{1}{\alpha_{air} A_{air}} \tag{3.44}$$

$$\alpha_{co} = f\left(\dot{m}_{co}, T_{HX,i}\right) \tag{3.45}$$

$$\alpha_{air} = f\left(\dot{m}_{air}, T_{air,i}\right) \tag{3.46}$$

$$\dot{m}_{air} = f\left(n, v_{vehicle}\right) \tag{3.47}$$

$$\Delta T = \frac{\Delta T_1 - \Delta T_2}{\ln\left(\frac{\Delta T_1}{\Delta T_2}\right)} \tag{3.48}$$

$$\Delta T_1 = T_{air,i} - T_{HX,o} \tag{3.49}$$

$$\Delta T_2 = T_{air,o} - T_{HX,o} \tag{3.50}$$

$$T_{air,o} = T_{air,i} + \left(1 - exp\left(-\frac{\alpha_{air} A_{ht,air}}{\dot{m}_{air} c_{p,air}}\right)\right)\left(T_w - T_{air,i}\right) \tag{3.51}$$

$$T_w = T_{HX,o} + R_{co}\dot{Q}_{HX} \tag{3.52}$$

$\dot{Q}_{HS}$ is the heating power of the conditioning unit, $\dot{Q}_{pipe1}$ and $\dot{Q}_{pipe2}$ represent the heat loss to the environment at the feeding and discharge pipe. $\dot{Q}_{HX}$ is the cooling capacity of the heat exchanger. $K = 67.57\frac{W}{K}$ denotes the product of thermal conductivity factor k_{pipe} and heat transfer area A_{pipe} of the feeding and discharge pipe to the ambient air with temperature $T_{air,i}$. The air mass flow $\dot{m}_{air}$ is a function of the fan's rotation speed n and the vehicle's driving speed $v_{vehicle}$.

Figure 3.2 displays the cooling circuit of the test bench setup, as it is

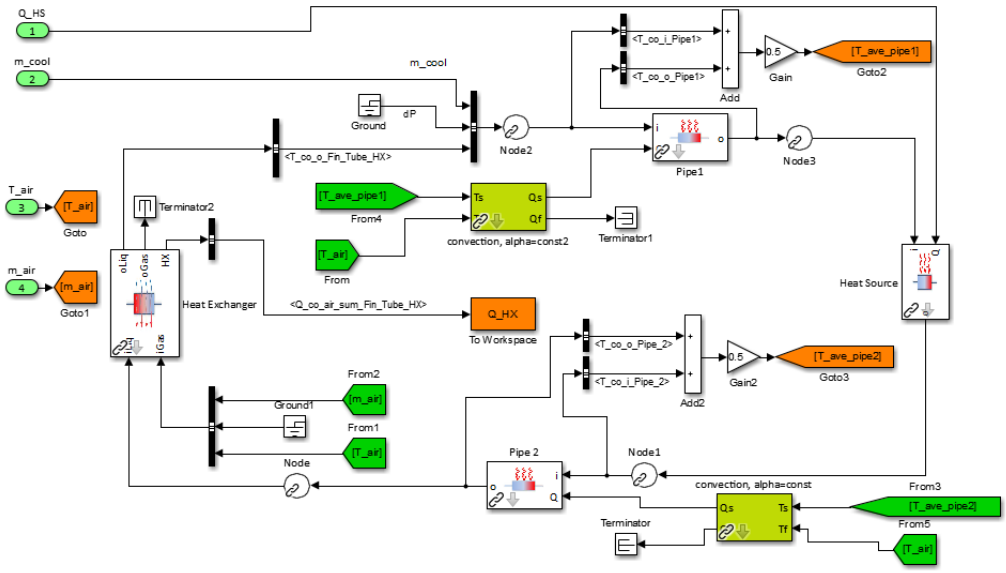

Figure 3.2: Simulink model of the cooling circuit

simulated in Simulink. The blocks are taken from the Thermo-Hydraulic Library [15].

4 Heat exchanger model - optimization

To ensure that the simulation shows the same cooling behaviour as the real heat exchanger, a two step unconstrained non-linear optimization of further parameters was done. In the first step the fin efficiency η, the tube free flow area $A_{flow,co}$ and the tube wetted perimeter P were optimized. The fin efficiency affects the convective heat transfer on the air side, as described in equation (3.28). The tube free flow area and the tube wetted perimeter both influence the coolant side of the heat exchanger as follows:

$$d_{hyd,co} = \frac{4A_{flow,co}}{P}, \tag{4.1}$$

$$Re_{co} = \frac{\dot{m}_{co,pertube} d_{hyd,co}}{A_{flow,o} \rho_{co} \nu_{co}}, \tag{4.2}$$

$$\alpha_{co} = \frac{Nu_{co} k_{co}}{d_{hyd,co}}. \tag{4.3}$$

In the second optimization step the three coefficients of equation (3.22) were optimized. As reference data the measurements from table 2.3 were taken.
The Optimization's cost function was implemented as the least mean squares of the error of the heat exchanger's cooling capacity. Due to the reason that the control strategy should work with coolant mass flows no higher than $8\frac{kg}{min}$, the relative error was taken for the cost function (4.4). In

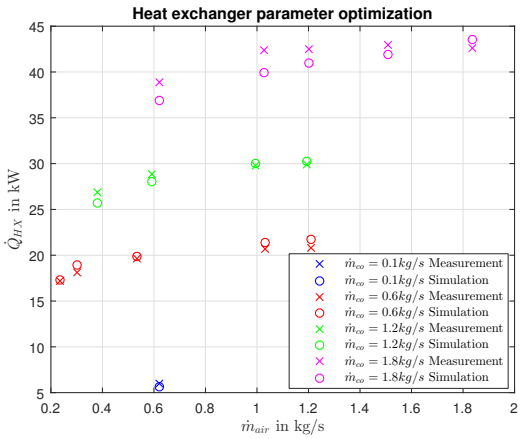

Figure 4.1: Simulation results of the optimized heat exchanger

Fin efficiency η	0.4587
Tube free flow area A_{flow}	$7.7047 \times 10^{-5} m^2$
Tube wetted perimeter P	$0.2848m$
a	0.1809
b	0.5038
c	0.0028

Table 4.1: Optimized parameters of the heat exchanger

that way the smaller coolant flows with less cooling capacity weight more in the optimization cost function.

$$J = \left(\frac{\dot{Q}_{HX} - \dot{Q}_{HX,Sim}}{\dot{Q}_{HX}} \right)^T \left(\frac{\dot{Q}_{HX} - \dot{Q}_{HX,Sim}}{\dot{Q}_{HX}} \right) \tag{4.4}$$

The reference cooling capacity $\dot{Q}_{HX}$ was calculated with equation (2.3). In Figure 4.1 and 4.2 the results of the optimization can be seen. It was possible to keep the relative simulation error beneath 7 per cent over the total range of coolant and air mass flow. The optimized parameter can be seen in table 4.1.

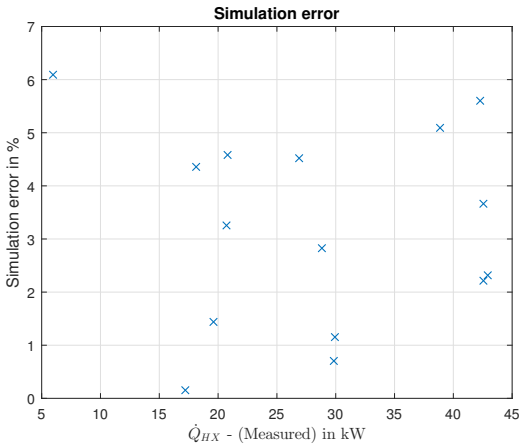

Figure 4.2: Simulation error of the optimized heat exchanger

To verify the simulation model, a comparative test was done. The measured coolant mass flow, air mass flow, air inlet temperature and heating power, from experiment No. 5 were fed into the optimized simulation model. Coolant inlet and outlet temperature as well as the cooling capacity of the heat exchanger were compared. The resulting plots can be seen in figure 4.3 and 4.4.

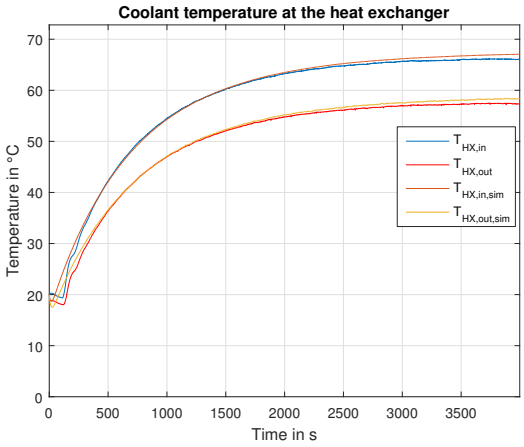

Figure 4.3: Coolant temperature at the heat exchanger, measured and simulated

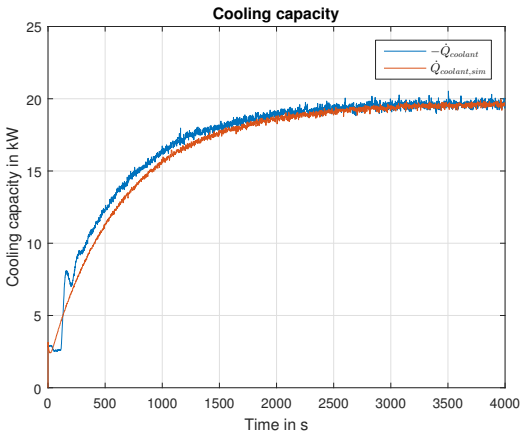

Figure 4.4: Cooling capacity of the heat exchanger, measured and simulated

5 Control strategy

5.1 Linearization

The mathematical model of the cooling circuit was transferred into the state space, by defining 4 state variables

$$\begin{aligned} x_1 &:= T_{HS,i}, \\ x_2 &:= T_{HS,o}, \\ x_3 &:= T_{HX,i}, \\ x_4 &:= T_{HX,o}. \end{aligned} \tag{5.1}$$

To keep the underlying model for the implemented control strategy as simple as possible, the plant model is split into a linear dynamic part and a nonlinear static part (Hammerstein model[10]).

5.1.1 Linear time-invariant state space model

The LTI-System has its orign in the equations (3.34) to (3.37). To receive a linear model, a few simplification had to be made. Firstly, the coolant mass flow is assumed to be constant. Secondly, all masses and specific heat capacities in the system are defined as temperature-independent and therefore are constant as well. The input parameter of the system is the cooling capacity of the heat exchanger $\dot{Q}_{HX}$. The heating power $\dot{Q}_{HS}$ as well as the air temperature $T_{air,i}$ are seen as uncontrollable input parameters.

So for a specific coolant mass flow, the linear part of the system can be described as follows:

$$\dot{\mathbf{x}} = \mathbf{A}\mathbf{x} + \mathbf{b}u + \mathbf{b}_{d1}d_1 + \mathbf{b}_{d2}d_2 \tag{5.2}$$

$$\mathbf{y} = \mathbf{C}\mathbf{x}, \tag{5.3}$$

with

$$\mathbf{x} = \begin{bmatrix} x_1 \\ x_2 \\ x_3 \\ x_4 \end{bmatrix}, \tag{5.4}$$

$$u = \dot{Q}_{HX}, \tag{5.5}$$

$$d_1 = \dot{Q}_{HS}, \tag{5.6}$$

$$d_2 = T_{air,i}, \tag{5.7}$$

$$\mathbf{A} = \begin{bmatrix} -\frac{\dot{m}_{co}}{m_{pipe1}} - \frac{K}{2m_{pipe1}\bar{c}_p} & 0 & 0 & \frac{\dot{m}_{co}}{m_{pipe1}} - \frac{K}{2m_{pipe1}\bar{c}_p} \\ \frac{\dot{m}_{co}}{m_{HS}} & -\frac{\dot{m}_{co}}{m_{HS}} & 0 & 0 \\ 0 & \frac{\dot{m}_{co}}{m_{pipe2}} - \frac{K}{2m_{pipe2}\bar{c}_p} & -\frac{\dot{m}_{co}}{m_{pipe2}} - \frac{K}{2m_{pipe2}\bar{c}_p} & 0 \\ 0 & 0 & \frac{\dot{m}}{m_{HX}} & -\frac{\dot{m}}{m_{HX}} \end{bmatrix}, \tag{5.8}$$

$$\mathbf{b} = \begin{bmatrix} 0 \\ 0 \\ 0 \\ \frac{1}{m_{HX}\bar{c}_p} \end{bmatrix}, \quad \mathbf{b}_{d1} = \begin{bmatrix} 0 \\ \frac{1}{m_{HS}\bar{c}_p} \\ 0 \\ 0 \end{bmatrix}, \quad \mathbf{b}_{d2} = \begin{bmatrix} \frac{K}{m_{pipe1}\bar{c}_p} \\ 0 \\ \frac{K}{m_{pipe2}\bar{c}_p} \\ 0 \end{bmatrix}, \tag{5.9}$$

As control variable for the MPC the coolant temperature of the heat source input x_1 is used, while the PI observer uses the state variables x_1, x_3 and x_4 as input. Therefore, the output vector used for the implementation of the Model Predictive Control $\mathbf{c}_{MPC}^T$ differs from the output matrix used for the observer implementation $\mathbf{C}_o$.

$$\mathbf{c}_{MPC}^{T} = \begin{bmatrix} 1 & 0 & 0 & 0 \end{bmatrix} \tag{5.10}$$

$$\mathbf{C}_o = \begin{bmatrix} 1 & 0 & 0 & 0 \\ 0 & 0 & 1 & 0 \\ 0 & 0 & 0 & 1 \end{bmatrix} \tag{5.11}$$

Due to the reason that the state variable x_4 is calculated as a byproduct of the heat exchanger inversion, it does not need to be measured but can be used as a virtual measurand. The two available coolant temperature sensors are used to measure x_1 and x_3.
In table 5.1 the used parameters for the linearization are illustrated.

$\bar{c}_p$	$3417.6\frac{J}{kgK}$
m_{pipe1}	$11.53kg$
m_{HS}	$69.13kg$
m_{pipe2}	$10.84kg$
m_{HX}	$3.05kg$
K	$67.57\frac{W}{K}$

Table 5.1: Parameters of the linearized model

This state space model only describes the cooling circuit for one specific coolant mass flow, as the dynamic matrix $\mathbf{A}$ depends on $\dot{m}_{co}$. For example, for a chosen coolant mass flow of $8\frac{kg}{min}$ the eigenvalues of the system are shown in table 5.2.

eigenvalues	
λ_1	-0.00039
λ_2	$-0.01346 + i0.0051$
λ_3	$-0.01346 - i0.0051$
λ_4	-0.04397

Table 5.2: Eigenvalue of the dynamic matrix $\mathbf{A}$ for $\dot{m}_{co} = 8\frac{kg}{min}$

5.2 Control design

The control design is implemented for a discrete, linear, time-invariant plant:

$$\begin{aligned} \mathbf{x}_{k+1} &= \mathbf{\Phi}\mathbf{x}_k + \mathbf{h}u_k + \mathbf{h}_{d1}d_{1,k} + \mathbf{h}_{d2}d_{2,k}, \\ y_{MPC,k} &= \mathbf{c}_{MPC}^T\mathbf{x}_k. \end{aligned} \tag{5.12}$$

The matrix $\mathbf{\Phi}$ and the vectors $\mathbf{h}$,$\mathbf{h}_{d1}$ and $\mathbf{h}_{d2}$ are derived from $\mathbf{A}$, $\mathbf{b}$, $\mathbf{b}_{d1}$, $\mathbf{b}_{d2}$ of equation (5.2) and the sampling time T_d as explained in [7]:

$$\mathbf{\Phi} = e^{\mathbf{A}T_d} \tag{5.13}$$

$$\mathbf{h} = \int_0^{T_d} e^{\mathbf{A}\tau}\mathbf{b}d\tau \tag{5.14}$$

$$\mathbf{h}_{d1} = \int_0^{T_d} e^{\mathbf{A}\tau}\mathbf{b}_{d1}d\tau \tag{5.15}$$

$$\mathbf{h}_{d2} = \int_0^{T_d} e^{\mathbf{A}\tau}\mathbf{b}_{d2}d\tau \tag{5.16}$$

The complete control concept for the cooling circuit exists of three separate parts:

- a Model Predictive Control to calculate the optimum cooling capacity,
- an observer to estimate all state variables and the heating power of the conditioning unit,
- a non-linear heat exchanger inversion to calculate the needed fan speed for a given cooling capacity and vehicle speed
- and a linear interpolation of the reference cooling capacities of two MPC's for different coolant mass flows.

In figures 5.1 and 5.2 the whole control concept is illustrated. The Model Predictive Control Interpolation's output is the reference cooling capacity

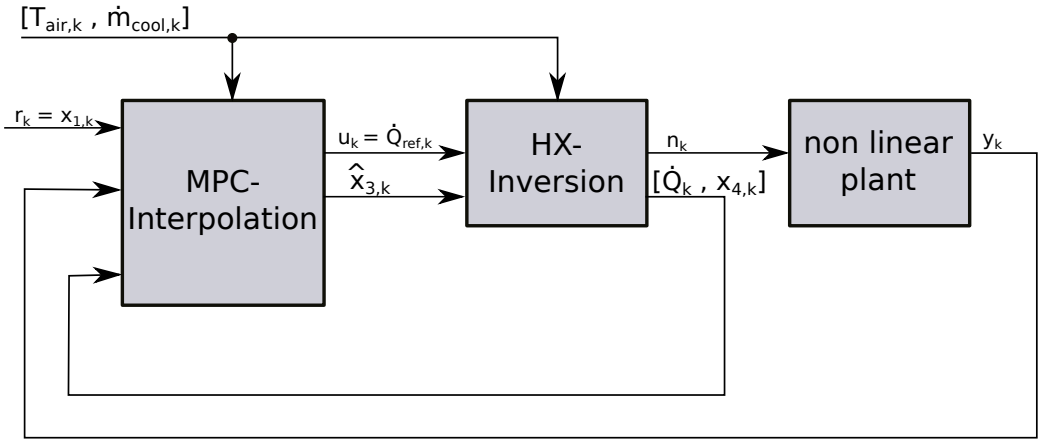

Figure 5.1: Control concept for a changing coolant mass flow

of the heat exchanger, which serves as input for the heat exchanger inversion. There, based on current coolant mass flow, coolant inlet temperature of the heat exchanger, vehicle speed and air temperature, a fan speed is calculated so that the cooling capacity of the heat exchanger model fits the reference signal. The PI observer estimates the states of the LTI system plus the heating power of the conditioning unit. As the calculation of the heat exchanger's coolant output temperature is a part of the heat exchanger-inversion, it can be added to the observer input as an additional virtual measurand.
Both MPC and PI observer are implemented twice for a minimum and a maximum coolant mass flow. Between these two, the optimal reference cooling capacity as well as the estimated heat exchanger's coolant inlet temperature are calculated by linear interpolation.

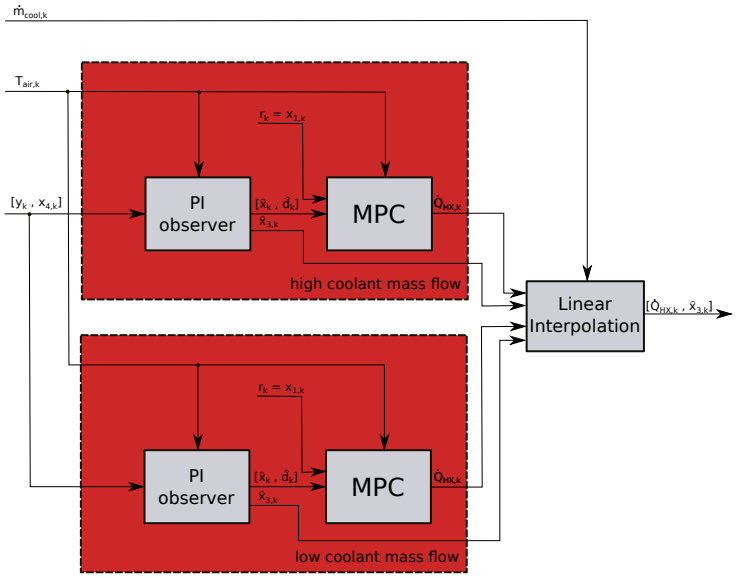

Figure 5.2: Linear interpolation

5.2.1 Model predictive control

The following objectives have to be fulfilled by the implemented control concept:

- Satisfaction of states and input constraints
- Minimization of control fault and maximization of performance in terms of control speed
- Possibility of real-time execution of an embedded system

A common way to receive an optimal control while satisfying all constraints is the Model Predictive Control (MPC), as explained in [1]. Taking into consideration that all state variables are available, the MPC calculates the control sequence for the control horizon N_c, so that the system behaviour is optimal in the prediction horizon N_p ($N_p \geq N_c$). The optimization is done with respect to all constraints, such as state, input and output constraints. From the resulting control output sequence, only the first sample is taken as control command, whilst the optimization is redone for the next time step. This leads to a so-called moving horizon

policy.
By defining r as the reference signal, one way to define the MPC problem is as follows:

$$\min_{\Delta u_{0,\dots,N_{c-1|k}}} \sum_{k=0}^{N_{p-1}} (r_k - y_{k|k})^2 Q + \sum_{k=0}^{N_{c-1}} \Delta u_{k|k}^2 R \tag{5.17}$$

w.r.t.

$$u_{k|k} = u_{k-1|k} + \Delta u_{k|k}, \quad (k = 0, 1, ..., N_{c-1}) \tag{5.18}$$

$$\mathbf{x}_{k+1|k} = \mathbf{\Phi}\mathbf{x}_{k|k} + \mathbf{h}u_{k|k} + \mathbf{h}_{d1}d_{1,k|k} + \mathbf{h}_{d2}d_{2,k|k}, \quad (k = 0, 1, ..., N_{p-1}) \tag{5.19}$$

$$y_{MPC,k|k} = \mathbf{c}_{MPC}^T \mathbf{x}_{k|k}, \quad (k = 0, 1, ..., N_{p-1}) \tag{5.20}$$

$$y_{MPC,k+1|k}^{\min} \leq y_{MPC,k+1|k} \leq y_{MPC,k+1|k}^{\max}, \quad (k = 0, 1, ..., N_{p-1}) \tag{5.21}$$

$$u_k^{\min} \leq u_{k|k} \leq u_k^{\max}, \quad (k = 0, 1, ..., N_{c-1}) \tag{5.22}$$

$$\Delta u_k^{\min} \leq \Delta u_{k|k} \leq \Delta u_k^{\max}, \quad (k = 0, 1, ..., N_{c-1}) \tag{5.23}$$

$$\Delta u_{k|k} = 0, \quad (N_c \leq k \leq N_p) \tag{5.24}$$

In this case, not the actual actuating variable but the change of it between two time steps is optimized. If $N_p > N_c$, the actuating variable is being held constant after passing the control horizon.

Unconstrained Model Predictive Control

In the unconstrained case the explicit solution of the optimization problem can be calculated. Therefore, the following matrices and vectors are defined:

$$\mathbf{y}_{MPC,k+1} = \begin{bmatrix} y_{MPC,k+1} \\ y_{MPC,k+2} \\ \cdot \\ \cdot \\ y_{MPC,k+N_p} \end{bmatrix}, \quad \mathbf{r}_{k+1} = \begin{bmatrix} r_{k+1} \\ r_{k+2} \\ \cdot \\ \cdot \\ r_{k+N_p} \end{bmatrix}, \quad \mathbf{\Delta u}_k = \begin{bmatrix} \Delta u_k \\ \Delta u_{k+1} \\ \cdot \\ \cdot \\ \Delta u_{k+N_c-1} \end{bmatrix} \tag{5.25}$$

$$\mathbf{F}_{MPC} = \begin{bmatrix} \mathbf{c}_{MPC}^T \mathbf{\Phi} \\ \mathbf{c}_{MPC}^T \mathbf{\Phi}^2 \\ . \\ . \\ \mathbf{c}_{MPC}^T \mathbf{\Phi}^{N_p} \end{bmatrix}, \tag{5.26}$$

$$\mathbf{g} = \begin{bmatrix} \mathbf{c}_{MPC}^T \mathbf{h} \\ \mathbf{c}_{MPC}^T (\mathbf{\Phi} + \mathbf{I}) \mathbf{h} \\ . \\ . \\ \mathbf{c}_{MPC}^T (\mathbf{\Phi}^{N_p - 1} + \cdots + \mathbf{\Phi} + \mathbf{I}) \mathbf{h} \end{bmatrix}, \tag{5.27}$$

$$\mathbf{g}_{d1} = \begin{bmatrix} \mathbf{c}_{MPC}^T \mathbf{h}_{d1} \\ \mathbf{c}_{MPC} (\mathbf{\Phi} + \mathbf{I}) \mathbf{h}_{d1} \\ . \\ . \\ \mathbf{c}_{MPC}^T (\mathbf{\Phi}^{N_p - 1} + \cdots + \mathbf{\Phi} + \mathbf{I}) \mathbf{h}_{d1} \end{bmatrix}, \tag{5.28}$$

$$\mathbf{g}_{d2} = \begin{bmatrix} \mathbf{c}_{MPC}^T \mathbf{h}_{d2} \\ \mathbf{c}_{MPC} (\mathbf{\Phi} + \mathbf{I}) \mathbf{h}_{d2} \\ . \\ . \\ \mathbf{c}_{MPC} (\mathbf{\Phi}^{N_p - 1} + \cdots + \mathbf{\Phi} + \mathbf{I}) \mathbf{h}_{d2} \end{bmatrix}, \tag{5.29}$$

$$\mathbf{L} = \begin{bmatrix} \mathbf{c}_{MPC}^T \mathbf{h} & \mathbf{0} & \cdots & \mathbf{0} \\ \mathbf{c}_{MPC}^T (\mathbf{\Phi} + \mathbf{I}) \mathbf{h} & \mathbf{c}_{MPC}^T \mathbf{h} & \cdots & \mathbf{0} \\ . & . & . & . \\ . & . & . & . \\ \mathbf{c}_{MPC}^T (\mathbf{\Phi}^{N_c - 1} + \cdots + \mathbf{\Phi} + \mathbf{I}) \mathbf{h} & \mathbf{c}_{MPC}^T (\mathbf{\Phi}^{N_c - 2} + \cdots + \mathbf{\Phi} + \mathbf{I}) \mathbf{h} & . & \mathbf{c}_{MPC}^T \mathbf{h} \\ . & . & . & . \\ . & . & . & . \\ \mathbf{c}_{MPC}^T (\mathbf{\Phi}^{N_p - 1} + \cdots + \mathbf{I}) \mathbf{h} & \mathbf{c}_{MPC}^T (\mathbf{\Phi}^{N_p - 2} + \cdots + \mathbf{I}) \mathbf{h} & . & \mathbf{c}_{MPC}^T (\mathbf{\Phi}^{N_p - N_c} + \cdots + \mathbf{I}) \mathbf{h} \end{bmatrix}, \tag{5.30}$$

where $\mathbf{I}$ is the identity matrix with the same rank as $\mathbf{\Phi}$. The system output can be described as

$$\mathbf{y}_{MPC,k+1} = \mathbf{F}_{MPC} \mathbf{x}_k + \mathbf{g} u_{k-1} + \mathbf{g}_{d1} d_{1,k-1} + \mathbf{g}_{d2} d_{2,k-1} + \mathbf{L} \mathbf{\Delta u}_k = \tilde{\mathbf{g}}_k + \mathbf{L} \mathbf{\Delta u}_k. \tag{5.31}$$

By defining

$$\mathbf{e}_k = \tilde{\mathbf{g}}_k - \mathbf{r}_{k+1} \tag{5.32}$$

the control fault can be written as

$$\mathbf{y}_{MPC,k+1} - \mathbf{r}_{k+1} = \mathbf{e}_k + \mathbf{L} \mathbf{\Delta u}_k, \tag{5.33}$$

which results in the optimization problem

$$\begin{aligned} J^\star &= \min_{\mathbf{\Delta u}_k}[(\mathbf{y}_{MPC,k+1} - \mathbf{r}_{k+1})^T\mathbf{Q}(\mathbf{y}_{MPC,k+1} - \mathbf{r}_{k+1}) + \mathbf{\Delta u}_k^T\mathbf{R}\mathbf{\Delta u}_k] = \\ &= \min_{\mathbf{\Delta u}_k}[\mathbf{\Delta u}_k^T(\mathbf{L}^T\mathbf{Q}\mathbf{L} + \mathbf{R})\mathbf{\Delta u}_k + 2\mathbf{\Delta u}_k^T\mathbf{L}^T\mathbf{Q}\mathbf{e}_k + \mathbf{e}_k^T\mathbf{Q}\mathbf{e}_k] \qquad (5.34) \\ \rightarrow \mathbf{\Delta u}_k^\star &= -(\mathbf{L}^T\mathbf{Q}\mathbf{L} + \mathbf{R})^{-1}\mathbf{L}^T\mathbf{Q}\mathbf{e}_k \qquad (5.35) \end{aligned}$$

If the weighting matrices $\mathbf{Q}$ and $\mathbf{R}$ are defined to be positive definite, the matrix inversion in equation (5.35) exists and $\mathbf{\Delta u}_k^\star$ is solvable. As only the first element of $\mathbf{\Delta u}_k^\star$ is used, the complete control law, for known $\mathbf{x}_{k-1}$, $d_{1,k-1}$, $d_{2,k-1}$ and u_{k-1}, can be finally written as:

$$\begin{aligned} \mathbf{x}_k &= \mathbf{\Phi}\mathbf{x}_{k-1} + \mathbf{h}u_{k-1} + \mathbf{h}_{d1}d_{1,k-1} + \mathbf{h}_{d2}d_{2,k-1} \qquad (5.36) \\ \mathbf{e}_k &= \tilde{\mathbf{g}}_k - \mathbf{r}_{k+1} \qquad (5.37) \\ \Delta u_k &= -\begin{bmatrix}1 & 0 & \dots & 0\end{bmatrix}(\mathbf{L}^T\mathbf{Q}\mathbf{L} + \mathbf{R})^{-1}\mathbf{L}^T\mathbf{Q}\mathbf{e}_k = -\mathbf{k}^T\mathbf{e}_k \qquad (5.38) \\ u_k &= u_{k-1} + \Delta u_k \qquad (5.39) \end{aligned}$$

Constrained Model Predictive Control

For a single input - single output (SISO) system, as it is in the present application, the constraints formulated in the equations (5.21) to (5.23) can easily be written as a system of inequalities:

$$\mathbf{W}\mathbf{\Delta u}_k \leq \mathbf{w} \qquad (5.40)$$

Therefore the following matrices have to be defined:

$$\mathbf{W} = \begin{bmatrix} -\mathbf{T} \\ \mathbf{T} \\ -\mathbf{U} \\ \mathbf{U} \\ -\mathbf{L} \\ \mathbf{L} \end{bmatrix}, \quad \mathbf{w} = \begin{bmatrix} -\mathbf{u}^{\min} + \mathbf{v}u_{k-1} \\ \mathbf{u}^{\max} - \mathbf{v}u_{k-1} \\ -\mathbf{\Delta u}^{\min} \\ \mathbf{\Delta u}^{\max} \\ -\mathbf{y}^{\min} + \tilde{\mathbf{g}}_k \\ \mathbf{y}^{\max} - \tilde{\mathbf{g}}_k \end{bmatrix}, \quad \mathbf{T} = \left.\begin{bmatrix} 1 & 0 & 0 & \dots & 0 \\ 1 & 1 & 0 & \dots & 0 \\ . & & & & \\ . & & & & \\ 1 & 1 & 1 & \dots & 1 \end{bmatrix}\right\} N_c \times N_c, \tag{5.41}$$

$$\mathbf{U} = \left.\begin{bmatrix} 1 & 0 & 0 & \dots & 0 & 0 \\ 0 & 1 & 0 & \dots & 0 & 0 \\ . & & & & & \\ . & & & & & \\ 0 & 0 & 0 & \dots & 0 & 1 \end{bmatrix}\right\} N_c \times N_c, \quad \mathbf{v} = \left.\begin{bmatrix} 1 \\ 1 \\ . \\ . \\ 1 \end{bmatrix}\right\} N_c \times 1, \tag{5.42}$$

and the constraints have to be written as vectors:

$$\mathbf{u}^{\min} = \begin{bmatrix} u_0^{\min} \\ . \\ . \\ u_{N_c-1}^{\min} \end{bmatrix}, \quad \mathbf{\Delta u}^{\min} = \begin{bmatrix} \Delta u_0^{\min} \\ . \\ . \\ \Delta u_{N_c-1}^{\min} \end{bmatrix}, \quad \mathbf{y}_{MPC}^{\min} = \begin{bmatrix} y_{MPC,1}^{\min} \\ . \\ . \\ y_{MPC,N_p}^{\min} \end{bmatrix}. \tag{5.43}$$

The same definitions apply, of course, to $\mathbf{u}^{\max}$,$\mathbf{\Delta u}^{\max}$ and $\mathbf{y}_{MPC}^{\max}$.

With these matrices the optimization problem for the *Constrained Model Predictive Control* is defined as:

$$\min_{\mathbf{\Delta u}_k} [\mathbf{\Delta u}_k^T (\mathbf{L}^T \mathbf{Q} \mathbf{L} + \mathbf{R}) \mathbf{\Delta u}_k + 2 \mathbf{\Delta u}_k^T \mathbf{L}^T \mathbf{Q} \mathbf{e}_k + \mathbf{e}_k^T \mathbf{Q} \mathbf{e}_k] \tag{5.44}$$

w.r.t.

$$\mathbf{W} \mathbf{\Delta u}_k \leq \mathbf{w} \tag{5.45}$$

Quadratic Programming for Inequality Constraints

The following approach to the Quadratic Programming for Inequaltiy Constraints is based on the books [17] and [8]. To be consistent with literature, the optimization problem is expressed as

$$J = \frac{1}{2}\mathbf{x}^T\mathbf{E}\mathbf{x} + \mathbf{x}^T\mathbf{f} \tag{5.46}$$

$$\mathbf{M}\mathbf{x} \leq \boldsymbol{\gamma}. \tag{5.47}$$

All matrices and vectors are assumed to be compatible in the quadratic programming problem. Additionally, $\mathbf{E}$ is assumed to be symmetric and positive definite. In contrast to quadratic programming for equality constraints, the number of constraints can be larger than the number of decision variables. Therefore, $\mathbf{M}\mathbf{x} \leq \boldsymbol{\gamma}$ may contain inactive and active constraints. A constraint is said to be inactive as long as $\mathbf{M}_i\mathbf{x} < \gamma_i$ applies. Thus, a constraint is active, if $\mathbf{M}_i\mathbf{x} = \gamma_i$ applies. $\mathbf{M}_i$ and γ_i represent the i-th row of $\mathbf{M}$, respectively the i-th element of $\boldsymbol{\gamma}$.
For further proceedings the *Lagrange multipliers* and the *Karush-Kuhn-Tucker conditions* have to be introduced.

Lagrange multipliers The method of Lagrange multipliers is a mathematical tool to find the local extrema of a function subject to equality constraints

$$J = \frac{1}{2}\mathbf{x}^T\mathbf{E}\mathbf{x} + \mathbf{x}^T\mathbf{f} \tag{5.48}$$

$$\mathbf{M}\mathbf{x} = \boldsymbol{\gamma}. \tag{5.49}$$

The original objective function J is extended to the Lagrange function

$$L(\mathbf{x}, \boldsymbol{\lambda}) = \frac{1}{2}\mathbf{x}^T\mathbf{E}\mathbf{x} + \mathbf{x}^T\mathbf{f} + \boldsymbol{\lambda}^T\left(\mathbf{M}\mathbf{x} - \boldsymbol{\gamma}\right), \tag{5.50}$$

where the vector $\boldsymbol{\lambda}$ contains the Lagrange multipliers λ_i. It is easy to see that the necessary conditions for the extended optimization problem are

$$\frac{\partial L}{\partial \mathbf{x}} = \mathbf{E}\mathbf{x} + \mathbf{f} + \mathbf{M}^T\boldsymbol{\lambda} = 0 \tag{5.51}$$

$$\frac{\partial L}{\partial \boldsymbol{\lambda}} = \mathbf{M}\mathbf{x} - \boldsymbol{\gamma} = 0. \tag{5.52}$$

The further calculation of the optimal solution for $\mathbf{x}$ and $\boldsymbol{\lambda}$ is straightforward.

Karush-Kuhn-Tucker conditions As the method of Lagrange multipliers only allows equality constraints, the Karush-Kuhn-Tucker (KKT) conditions are introduced:

$$\mathbf{E}\mathbf{x} + \mathbf{f} + \mathbf{M}^T\boldsymbol{\lambda} = 0 \tag{5.53}$$

$$\mathbf{M}\mathbf{x} - \boldsymbol{\gamma} \leq 0 \tag{5.54}$$

$$\boldsymbol{\lambda}\left(\mathbf{M}\mathbf{x} - \boldsymbol{\gamma}\right) = 0 \tag{5.55}$$

$$\boldsymbol{\lambda} \leq 0. \tag{5.56}$$

To satisfy equation (5.55) $\lambda_i \stackrel{!}{=} 0$ if $\mathbf{M}_i\mathbf{x} < \gamma_i$ (which means that the i-th constraint is inactive). By defining S_{act} as the index set of active constraints, the KKT conditions can be written as:

$$\mathbf{E}\mathbf{x} + \mathbf{f} + \sum_{i \in S_{act}} \lambda_i \mathbf{M}_i^T = 0 \tag{5.57}$$

$$\mathbf{M}_i\mathbf{x} - \gamma_i = 0 \quad i \in S_{act} \tag{5.58}$$

$$\mathbf{M}_i\mathbf{x} - \gamma_i < 0 \quad i \notin S_{act} \tag{5.59}$$

$$\lambda_i \geq 0 \quad i \in S_{act} \tag{5.60}$$

$$\lambda_i = 0 \quad i \notin S_{act}. \tag{5.61}$$

As it can be seen in equations (5.60) and (5.61), the Lagrange multiplier is zero if the corresponding constraint is inactive, and non-negative if the constraint is active. Therefore, if the active set is known, the original problem with inequality constraints can be replaced by an optimization problem with only equality constraints. For this alternative problem, the optimal solution is

$$\boldsymbol{\lambda}_{act} = -\left(\mathbf{M}_{act}\mathbf{E}^{-1}\mathbf{M}_{act}^{T}\right)^{-1}\left(\boldsymbol{\gamma}_{act} + \mathbf{M}_{act}\mathbf{E}^{-1}\mathbf{f}\right) \tag{5.62}$$

$$\mathbf{x} = -\mathbf{E}^{-1}\left(\mathbf{f} + \mathbf{M}_{act}^{T}\boldsymbol{\lambda}_{act}\right). \tag{5.63}$$

The main difficulty in solving a quadratic program with inequality constraints is to find the right set of active constraints. All further steps are straight forward, as described in equations (5.62) and (5.63). To find these active constraints and the corresponding Lagrange multipliers, the Primal-Dual Method is used.

Prime-Dual Method This method is based on two optimization problems. The primal problem which is the original problem with inequality constraints (5.46) and the so-called dual problem. In the dual problem, the Lagrange multipliers are used as decision variables, and therefore are called dual variables in literature. By using this method, the inactive constraints can be systematically identified and eliminated from the solution. If a feasible solution exists, the original (primal) problem can be written as

$$\max_{\boldsymbol{\lambda}\geq\mathbf{0}} \min_{\mathbf{x}} \left[\frac{1}{2}\mathbf{x}^{T}\mathbf{E}\mathbf{x} + \mathbf{x}^{T}\mathbf{f} + \boldsymbol{\lambda}^{T}\left(\mathbf{M}\mathbf{x} - \boldsymbol{\gamma}\right)\right]. \tag{5.64}$$

As the problem is unconstrained, the solution for x is equivalent to (5.63)

$$\mathbf{x} = -\mathbf{E}^{-1}\left(\mathbf{F} + \mathbf{M}^{T}\boldsymbol{\lambda}\right). \tag{5.65}$$

By substituting $\mathbf{x}$ in (5.64), the dual problem is defined as

$$\min_{\lambda \geq \mathbf{0}} \left(\frac{1}{2} \lambda^T \tilde{\mathbf{H}} \lambda + \lambda^T \tilde{\mathbf{k}} + \frac{1}{2} \gamma^T \mathbf{E}^{-1} \gamma \right) \tag{5.66}$$

with the given matrices $\tilde{\mathbf{H}}$ and $\tilde{\mathbf{k}}$

$$\tilde{\mathbf{H}} = \mathbf{M} \mathbf{E}^{-1} \mathbf{M}^T \tag{5.67}$$

$$\tilde{\mathbf{k}} = \gamma + \mathbf{M} \mathbf{E}^{-1} \mathbf{f}. \tag{5.68}$$

The optimal set of dual variables that minimizes (5.66) is identified as the active set of Lagrange multipliers λ_{act}, with the corresponding matrix $\mathbf{M}_{act}$ and vector γ_{act}. By using this active set of constraints, the solution for the primal variable $\mathbf{x}$ (5.65) becomes (5.63).

Hildreth's Solver for Quadratic Problems In [6] and [5] a simple algorithm to solve the dual problem is proposed. The algorithm starts with any feasible set of Lagrange multipliers $\lambda^0 \geq \mathbf{0}$ and calculates the dual variables for the next iteration step component-by-component. To reach this goal the dual objective function

$$\varphi(\lambda) = \frac{1}{2} \lambda^T \tilde{\mathbf{H}} \lambda + \lambda^T \tilde{\mathbf{k}} + \frac{1}{2} \gamma^T \mathbf{E}^{-1} \gamma \tag{5.69}$$

is being minimized separately for each component λ_i, with respect to $\lambda_i \geq 0$, while all other Lagrange multipliers are kept constant at their last value. This leads to the iterative algorithm

$$\lambda_i^{p+1} = \max \left\{ 0, w_i^{p+1} \right\} \tag{5.70}$$

with

$$w_i^{p+1} = -\frac{1}{\tilde{h}_{ii}} \left[\tilde{k}_i + \sum_{j=1}^{i-1} \tilde{h}_{ij} \lambda_j^{p+1} + \sum_{j=i+1}^{n} \tilde{h}_{ij} \lambda_j^p \right], \tag{5.71}$$

where $\tilde{h}_{ij}$ is the ij-th element of (5.67) and $\tilde{k}_i$ is the i-th element of (5.68). Equation (5.71) is obtained by setting the derivative

$$\frac{\partial \varphi}{\partial \lambda_i} = \sum_{j=1}^{n} \tilde{h}_{ij} \lambda_j + \tilde{k}_i \tag{5.72}$$

zero and insert the already calculated values λ_j^{p+1} for $j < i$ and λ_j^p for $j > i$. It can be said that $\varphi(\boldsymbol{\lambda}^p)$ converges to $\varphi^{min} = \varphi(\boldsymbol{\lambda}^\star)$ and $\mathbf{x}(\boldsymbol{\lambda}^p)$ converges to $\mathbf{x}^\star = \mathbf{x}(\boldsymbol{\lambda}^\star)$. The proof of the convergence is shown in [8].

```
function Delta_uk = hildreth(L,Q,R,ek,W,w)
%#eml

%Matrices for Hildreth-solver
E = 2*(L'*Q*L+R);
F = 2*L'*Q*ek;
M=W;
gamma=w;

% Hildreth-solver
[n1,m1] = size(M);
Delta_uk = -E\F;
Delta_uk = Delta_uk(:);
kk = 0;
for i = 1:n1
    if (M(i,:)*Delta_uk > gamma(i))
        kk = kk+1;
    else
        kk = kk+0;
    end
end
if kk ~= 0
        H = M*(E\M');
        K = (M*(E\F)+gamma);
    [n,m] = size(K);
    x_ini = zeros(n,m);
    lambda = x_ini;
    for km = 1:80
        lambda_p = lambda;
        for i = 1:n
            w=-(K(i,1)+H(i,:)*lambda-H(i,i)*lambda(i,1))/H(i,i);
            lambda(i,1) = max(0,w);
        end
        al = (lambda-lambda_p)'*(lambda-lambda_p);
        if (al<10e-8);
            break;
        end
    end
    Delta_uk = -E\F -E\M'*lambda;
end
```

The code above shows the implemented Hildreth solver in *Matlab* [17]. The matrices and vectors, which are defined for the Constrained MPC in (5.44), are passed to the function as input arguments. The return value of the function is the optimal control sequence $\mathbf{\Delta u}_k^\star$. As the computation of the Lagrange multipliers is done component-by-component, no matrix inversion is needed. Therefore, if the set of active constraints is feasible when treated as equality constraints, the Lagrange multipliers will converge. However, if the active constraints are not linearly independent or their number is greater than the number of decision variables, the dual variables will not converge to a fixed value. But due to the lack of a matrix inversion, the algorithm will continue without interruption. In [17] it is shown that even if the active set of constraints is not feasible, the Hildreth solver will compute a compromised, near-optimal solution. The feature to recover from ill-conditioned constraints is also a main reason to choose this algorithm for real-time applications.
For the implementation of the Model Predictive Control the following parameters were used:

Description	Variable	Value	Unit
Sample time	T_{MPC}	4	s
Maximum actuating variable	u_{max}	0	kW
Minimum actuating variable	u_{min}	-30	kW
Maximum actuating variable changing rate	Δu_{max}	400	$\frac{W}{\text{Time step}}$
Minimum actuating variable changing rate	Δu_{min}	-400	$\frac{W}{\text{Time step}}$
Maximum control variable	y_{max}	40.5	$^\circ C$
Minimum control variable	y_{min}	25	$^\circ C$
Diagonal elements of the weighting matrix $\mathbf{Q}$	Q_i	10^9	-
Diagonal elements of the weighting matrix $\mathbf{R}$	R_i	1	-
Control horizon	N_c	4	Time steps
Prediction horizon	N_p	35	Time steps

Table 5.3: Parameters of the implemented MPC

5.2.2 Proportional-integral (PI) observer

The designed Constrained Model Predictive Control does not only need all states of the LTI model but also the heating power of the conditioning unit as disturbance variable. Due to the assumption that the waste heat of a vehicle engine is not known, the heating power is estimated. Therefor, a so-called proportional integral observer (PI observer), applied and developed in [13], is used. The PI observer is an extension to the classical Luenberger observer [9].
The implemented observer does not only get the state variables x_1 and x_3 but also the state variable x_4, as it can be seen in figure 5.1. x_4 is calculated in the heat exchanger inversion part of the complete control strategy and is therefore seen as a virtual measured variable in the observer model. For the existing plant described in equation (5.12), the output matrix $\mathbf{c}_{MPC}^T$ is changed to $\mathbf{C}_o$, which is defined in equation (5.11). The resulting system can is described with equation (5.73) and (5.74). This leads to the description:

$$\mathbf{x}_{k+1} = \mathbf{\Phi}\mathbf{x}_k + \mathbf{h}u_k + \mathbf{h}_{d1}d_{1,k} + \mathbf{h}_{d2}d_{2,k}, \tag{5.73}$$

$$\mathbf{y}_{o,k} = \mathbf{C}_o\mathbf{x}_k. \tag{5.74}$$

The Luenberger observer would eventually reach its performance limits, as the heat source's heating power is a slowly varying disturbance $d_{1,k}$ and produces a persistent estimation error. The PI observer avoids that by estimating the unknown disturbance variable and treating it like a known input to the observer model. By doing so, not only the estimated variable $\hat{d}_{1,k}$ is available to the control algorithm, but also the performance of the state estimation is improved, as there is no longer a permanent observer error. The structue of the time discrete PI observer is illustrated in figure 5.3.

For the design of the observer, the unknown inputs are treated as additional state variables which increases the order of the observer model by the number of unknown inputs. The corresponding system of differential equations is:

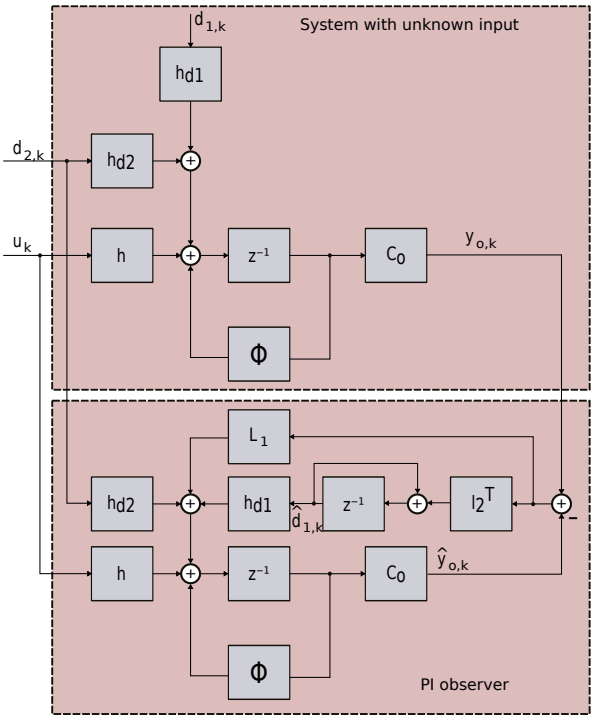

Figure 5.3: Structure of the PI observer

$$\begin{bmatrix} \hat{\mathbf{x}}_{k+1} \\ \hat{d}_{1,k+1} \end{bmatrix} = \underbrace{\begin{bmatrix} \mathbf{\Phi} & \mathbf{h}_{d1} \\ 0 & 1 \end{bmatrix}}_{\mathbf{\Phi}_e} \begin{bmatrix} \hat{\mathbf{x}}_k \\ \hat{d}_{1,k} \end{bmatrix} + \underbrace{\begin{bmatrix} \mathbf{h} \\ 0 \end{bmatrix}}_{\mathbf{h}_e} u_k + \underbrace{\begin{bmatrix} \mathbf{h}_{d2} \\ 0 \end{bmatrix}}_{\mathbf{h}_{d2,e}} d_{2,k} + \underbrace{\begin{bmatrix} \mathbf{L}_1 \\ \mathbf{l}_2^T \end{bmatrix}}_{\mathbf{L}_e} \left(\mathbf{y}_{o,k} - \hat{\mathbf{y}}_{o,k} \right), \tag{5.75}$$

$$\hat{\mathbf{y}}_{o,k} = \underbrace{\begin{bmatrix} \mathbf{C}_o & \mathbf{0} \end{bmatrix}}_{\mathbf{C}_e} \begin{bmatrix} \hat{\mathbf{x}}_k \\ \hat{d}_{1,k} \end{bmatrix}. \tag{5.76}$$

The estimation error of the observer is defined as

$$\mathbf{e}_{e,k} = \begin{bmatrix} \mathbf{x}_k \\ d_{1,k} \end{bmatrix} - \begin{bmatrix} \hat{\mathbf{x}}_k \\ \hat{d}_{1,k} \end{bmatrix}, \tag{5.77}$$

and therefore, the dynamic of the estimation error can be written as

$$\mathbf{e}_{e,k+1} = \begin{bmatrix} \mathbf{x}_{k+1} \\ d_{1,k+1} \end{bmatrix} - \begin{bmatrix} \hat{\mathbf{x}}_{k+1} \\ \hat{d}_{1,k+1} \end{bmatrix} \tag{5.78}$$

$$= \mathbf{\Phi}_e \begin{bmatrix} \mathbf{x}_k \\ d_k \end{bmatrix} + \mathbf{h}_e u_k + \mathbf{h}_{d2,e} d_{2,k} - \mathbf{\Phi}_e \begin{bmatrix} \hat{\mathbf{x}}_k \\ \hat{d}_{1,k} \end{bmatrix} - \mathbf{h}_e u_k - \mathbf{h}_{d2,e} d_{2,k} - \mathbf{L}_e \mathbf{C}_e \mathbf{e}_{e,k} \tag{5.79}$$

$$= \left(\mathbf{\Phi}_e - \mathbf{L}_e \mathbf{C}_e \right) \mathbf{e}_{e,k}. \tag{5.80}$$

The feedback matrix $\mathbf{L}_e$ can be derived from the LQR (Linear-quadratic Regulator) state feedback matrix of the corresponding dual plant. The LQR with infinite time horizon for discrete time systems solves the optimization problem

$$\min_{\mathbf{u}_k} \left(\sum_{k=0}^{\infty} \mathbf{x}_k^T \mathbf{Q}_{LQR} \mathbf{x}_k + u_k R_{LQR} u_k \right) \tag{5.81}$$

w.r.t

$$\mathbf{x}_{k+1} = \mathbf{\Phi}_e \mathbf{x}_k + \mathbf{h}_e u_k \tag{5.82}$$

$$u_k = -\mathbf{k}_{LQR}^T \mathbf{x}_k. \tag{5.83}$$

The solution of the optimization problem is

$$\mathbf{k}_{LQR}^T = \left(R_{LQR} + \mathbf{h}_e^T \mathbf{P}_{LQR} \mathbf{h}_e \right)^{-1} \mathbf{h}_e^T \mathbf{P}_{LQR} \mathbf{\Phi}_e, \tag{5.84}$$

where $\mathbf{P}_{LQR}$ is the unique, positive definite solution of the discrete time algebraic Riccati equation (DARE)

$$\mathbf{P}_{LQR} = \mathbf{\Phi}_e^T \mathbf{P}_{LQR} \mathbf{\Phi}_e - \mathbf{\Phi}_e^T \mathbf{P}_{LQR} \mathbf{h}_e \left(R_{LQR} + \mathbf{h}_e^T \mathbf{P}_{LQR} \mathbf{h}_e \right)^{-1} \mathbf{h}_e^T \mathbf{P}_{LQR} \mathbf{\Phi}_e + \mathbf{Q}_{LQR}. \tag{5.85}$$

By substituting

$$\mathbf{\Phi}_e \rightarrow \mathbf{\Phi}_e^T \tag{5.86}$$

$$\mathbf{h}_e \rightarrow \mathbf{C}_e^T \tag{5.87}$$

$$\mathbf{k}_{LQR} \rightarrow \mathbf{L}_e^T \tag{5.88}$$

$$\mathbf{Q}_{LQR} \rightarrow \mathbf{Q}_{LQE} \tag{5.89}$$

$$R_{LQR} \rightarrow \mathbf{R}_{LQE} \tag{5.90}$$

the observer's feedback matrix $\mathbf{L}_e$ can be calculated according to equations (5.84) and (5.85).
The following sample time and weighting matrices were used for the observer implementation:

$$T_{d,observer} = 0.2s \tag{5.91}$$

$$\mathbf{Q}_{LQE} = \begin{bmatrix} 10 & 0 & 0 & 0 & 0 \\ 0 & 10^{-4} & 0 & 0 & 0 \\ 0 & 0 & 1 & 0 & 0 \\ 0 & 0 & 0 & 1 & 0 \\ 0 & 0 & 0 & 0 & 10^{6} \end{bmatrix} \tag{5.92}$$

$$\mathbf{R}_{LQE} = \begin{bmatrix} 10^{3} & 0 & 0 \\ 0 & 10^{3} & 0 \\ 0 & 0 & 10^{3} \end{bmatrix} \tag{5.93}$$

Comparison Luenberger observer to PI observer

For both observers the feedback matrix has been calculated the same way as described above. While the PI observer additionally estimates the heating power of the conditioning unit $\hat{d}_1$, the Luenberg observer only estimates the four state variables. The measured values are generated by the non-linear simulation model as illustrated in figure 3.2, with the difference that the cooling power of the heat exchanger u_k was fed directly to the model as an input variable. Also the simulated state space variables x_1, x_3 and x_4 were overlapped with a white noise $w\ \epsilon[-0.3, 0.3]$. The Luenberger observer was designed with the weighting matrices

$$\mathbf{Q}_{LQE,Luenberger} = \begin{bmatrix} 10 & 0 & 0 & 0 \\ 0 & 10^{-4} & 0 & 0 \\ 0 & 0 & 1 & 0 \\ 0 & 0 & 0 & 1 \end{bmatrix} \tag{5.94}$$

$$\mathbf{R}_{LQE,Luenberger} = \begin{bmatrix} 10^{3} & 0 & 0 \\ 0 & 10^{3} & 0 \\ 0 & 0 & 10^{3} \end{bmatrix}. \tag{5.95}$$

For the whole simulation time, the coolant mass flow was held on a constant value, for which also the two observers were implemented. In figure

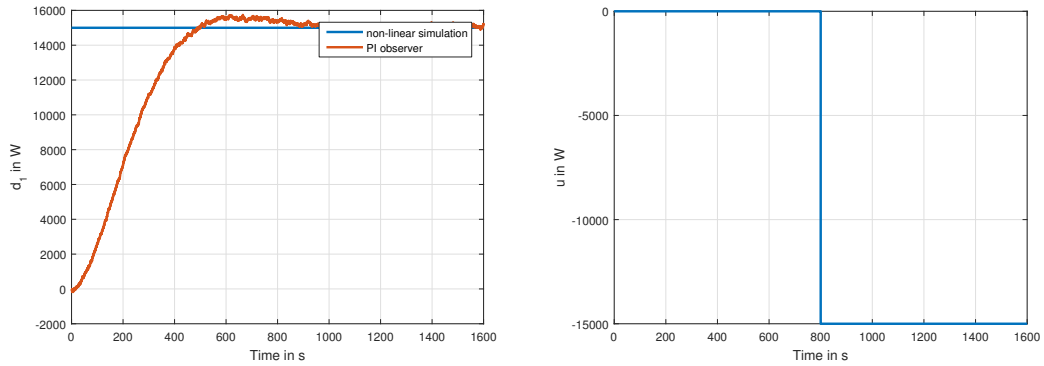

Figure 5.4: Input variables for the observer comparison

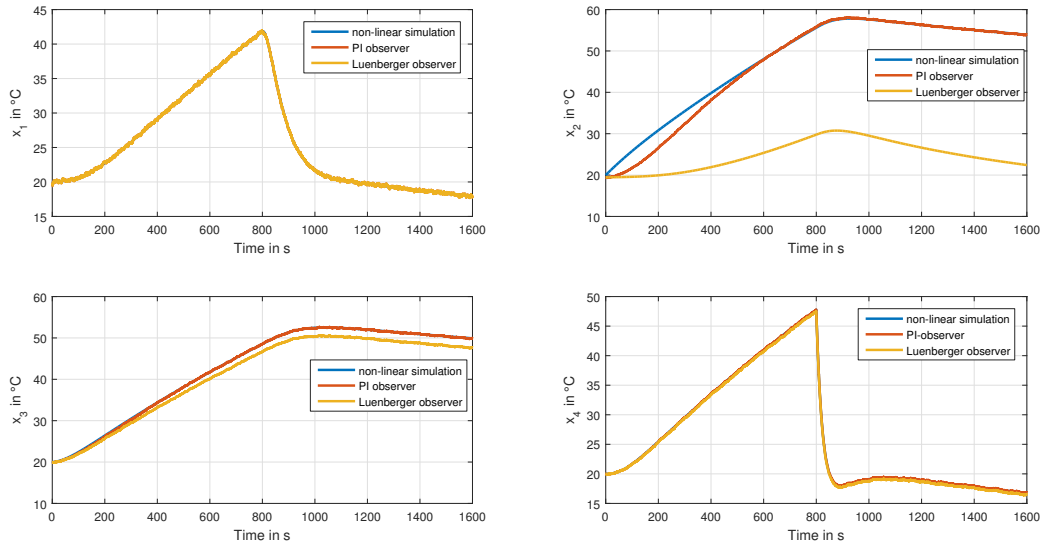

Figure 5.5: Estimated state variables

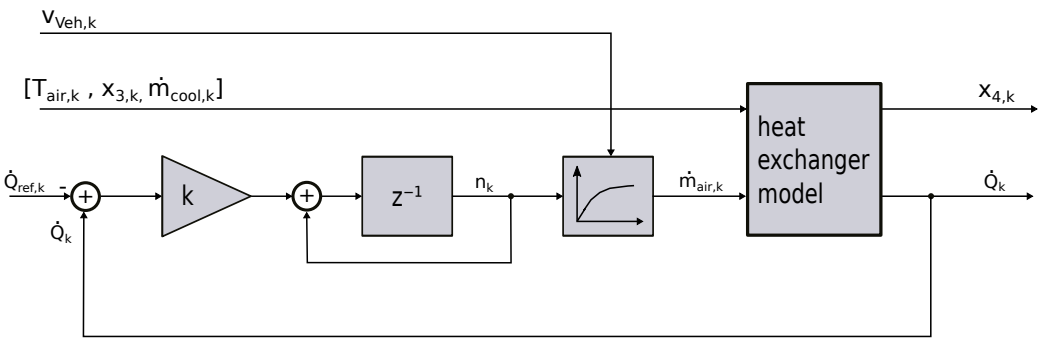

Figure 5.6: Heat exchanger inversion

5.4 the input variables u and d_1 to the nonlinear system and additionally the estimated value for $\hat{d}_1$ are illustrated. Figure 5.5 shows all estimated state variables for the Luenberg observer and the PI observer. Especially for the state variable x_2 the advantage of the PI observer compared to the Luenberger observer can be seen.

5.2.3 Heat exchanger inversion

As the MPC only provides the optimal cooling power for the heat exchanger, the corresponding fan speed n_k has to be calculated afterwards. This is done by a simple integrator, a look-up table to match the fan speed to a corresponding air mass flow and a model of the heat exchanger. The structure of the heat exchanger inversion can be seen in figure 5.6.
The heat exchanger model calculates for given mass flow and inlet temperature of coolant and air the associated cooling power according to equations (3.37) and (3.41) to (3.52). As a byproduct the coolant outlet temperature of the heat exchanger $x_{4,k}$ is calculated. Both the calculated cooling power and the coolant outlet temperature of the heat exchanger serve as actuating variable u_k respectively as virtually measured state space variable $x_{4,k}$ for the observer.

5.2.4 MPC Interpolation

As can be seen in figure 5.2 the reference cooling capacity for the heat exchanger inversion is generated by the linear interpolation of the outputs of two MPC's. This was necessary as the cooling pump does not generate a constant coolant mass flow. If only one MPC with fixed coolant mass flow would be implemented, it could lead to a control deviation or oscillation. In figure 5.7 two MPC strategies are compared. The non-linear plant (figure 3.2) was being operated with constant coolant mass flow $\dot{m}_{cool} = 8\frac{kg}{min}$, air temperature $T_{air} = 22°C$, heating power $\dot{Q}_{HS} = 15kW$ and set-point temperature $x_{1,set} = 40°C$. For the Interpolated MPC two Model Predictive Controls, $\dot{m}_{cool,low} = 5\frac{kg}{min}$ and $\dot{m}_{cool,high} = 15\frac{kg}{min}$, are designed, while for the second control strategy the MPC was implemented for a coolant mass flow of $\dot{m}_{cool} = 5\frac{kg}{min}$.
As it can be seen in figure 5.7, the Interpolated MPC regulates the coolant temperature at the heat source intake without control deviation or overshooting. In contrast to that, the MPC implemented with the wrong coolant mass flow oscillates around the temperature set-point and does not progress into a steady state even after $50min$.

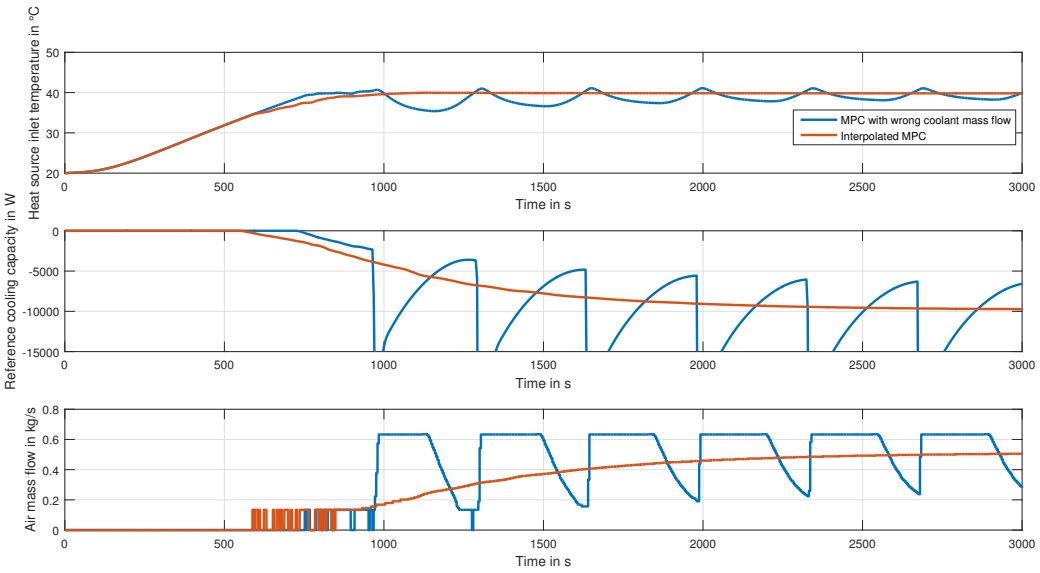

Figure 5.7: Comparision of one MPC to two Interpolated MPC's at $\dot{m}_{cool} = 8\frac{kg}{min}$

6 Results

6.1 Comparison of test bench setup to simulation

The implemented Model Predictive Control and PI observer plus the MPC Interpolation were tested at the test bench and compared to the simulation model. Figure 6.1 shows the, at the test bench measured, air temperature and coolant mass flow during the ongoing experiment. Since the conditioning unit of the test bench was being operated at the lowest possible coolant mass flow, neither the mass flow, nor the heating power could be held constant. Additionally, the actual heating power can not be measured. Therefore, the heating power that is used in the simulation model, had to be estimated by observing the heat source outlet temperature, respectively the heat exchanger inlet temperature. Due to the reason that the coolant mass flow is quite low, the heating elements in the conditioning unit were switched off during the heating process to prevent over-heating. In figure 6.1 the used heating power in the simulation is shown.
Additionally, the factor K from equation (3.39) and (3.40) had to be adjusted in the simulation model, as the heat loss in the pipes is not only a function of the surrounding air temperature but also of the floor temperature, since the pipes were lying on the floor uninsulated. Therefore, K was increased by 20%. As it can be seen in figure 6.2 the simulation fits well to the measured data. The only difference between the measured data and simulation is in the coolant inlet temperature of the heat source. This can be explained by unmodelled masses of pipes and metal junctions.

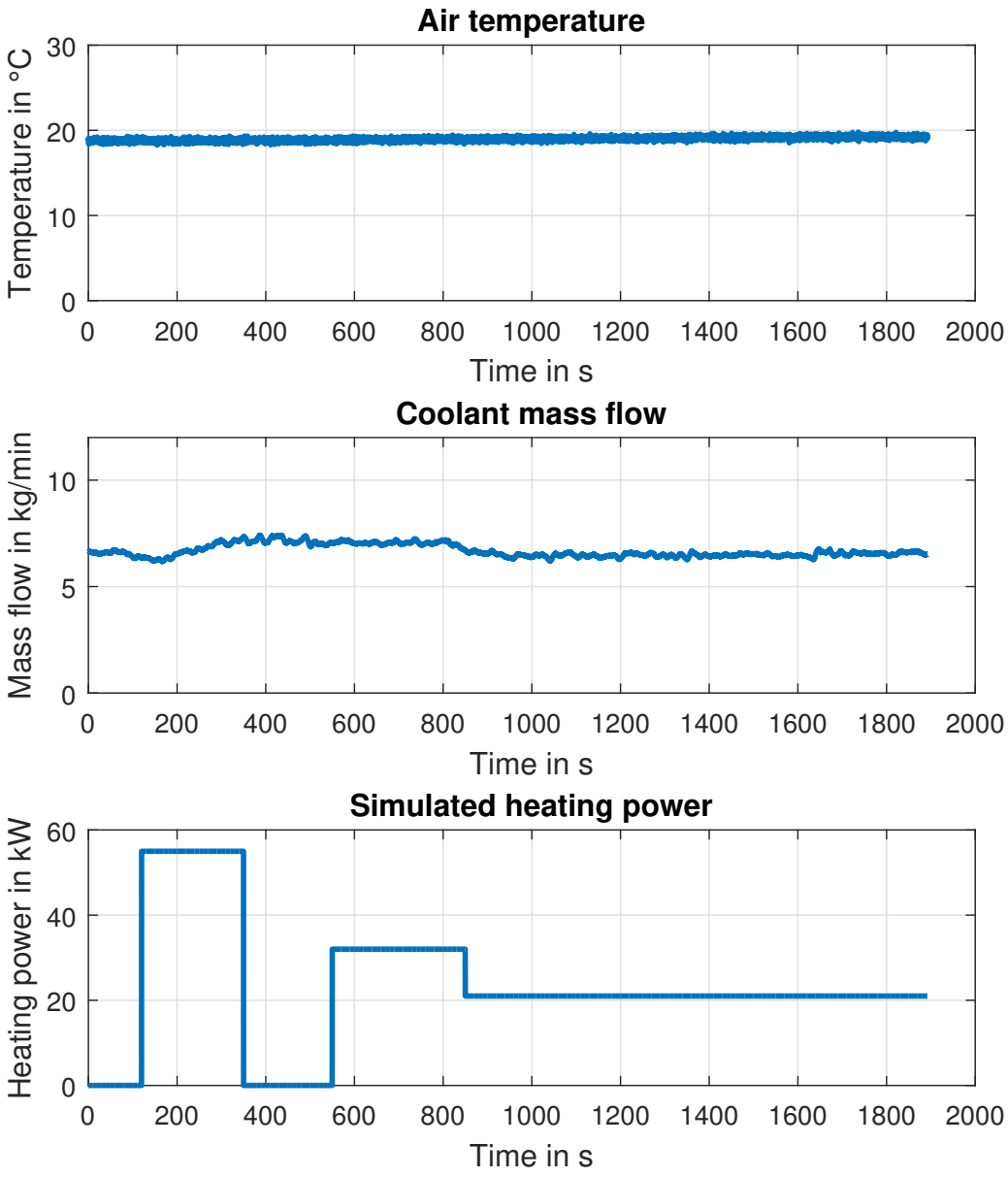

Figure 6.1: Input data for the simulation

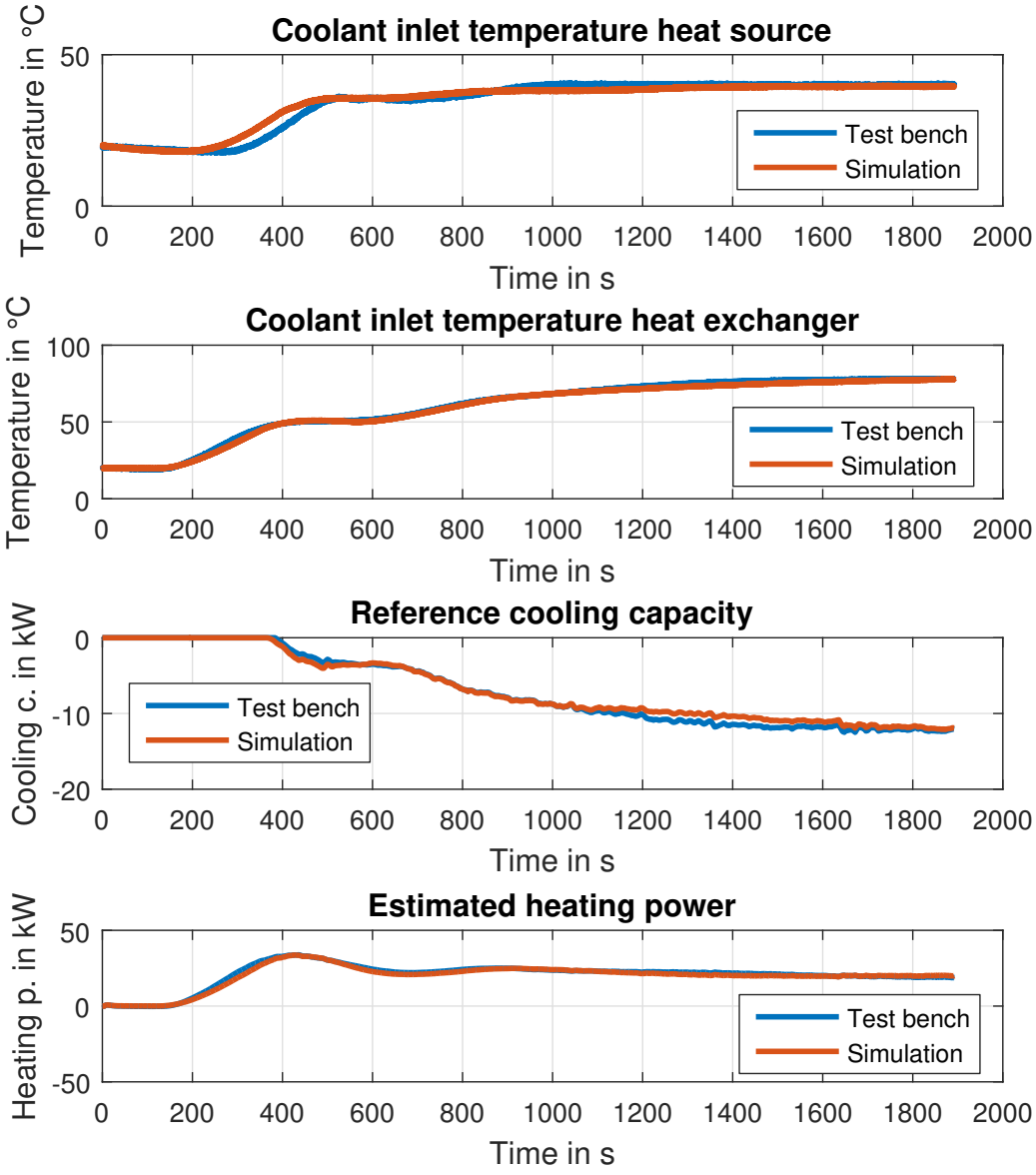

Figure 6.2: Comparison of test bench to simulation

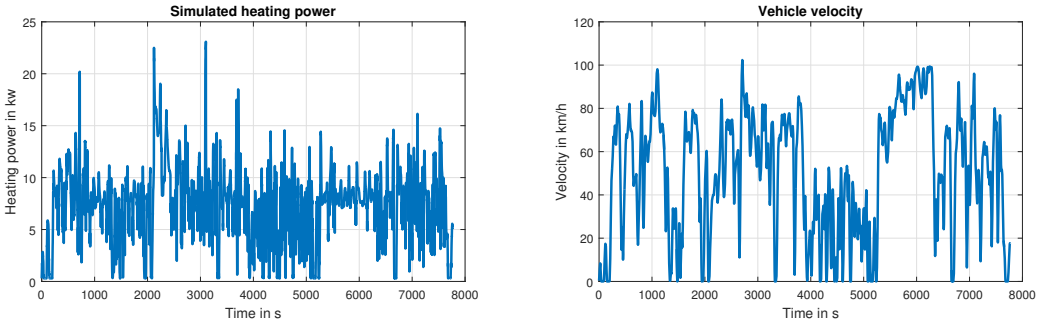

Figure 6.3: Simulation data

6.2 Comparison bang-bang control to MPC

When comparing the bang-bang control and MPC the heat loss of a real life cycle of an electric vehicle were used as simulated heating power. In figure 6.3 the simulated heating power as well as the simulated vehicle velocity is displayed.
For the bang-bang control strategy a four point control with hysteresis was used. The control gets the coolant inlet temperature of the heat source as input signal and provides the duty factor of pulses for the fan drive as output signal, which is shown in figure 6.4.Both simulations used fixed coolant mass flow and air temperature.

Air temperature	$30°C$
Coolant mass flow	$7\frac{kg}{min}$

Table 6.1: Fixed simulation parameters

In figure 6.5 the results of the two control strategies are illustrated. As it can be observed, the Model Predictive Control is able to keep a steady coolant temperature at the heat source inlet, although the vehicle velocity varies between $0\frac{km}{h}$ and $100\frac{km}{h}$ and the introduced heating power varies between $0.3kW$ and $23kW$. In contrast to the MPC the bang-bang control keeps the coolant temperature much less constant. Additionally, the energy consumed by the cooling fan is about 75% higher when using a bang-bang control instead of the MPC.

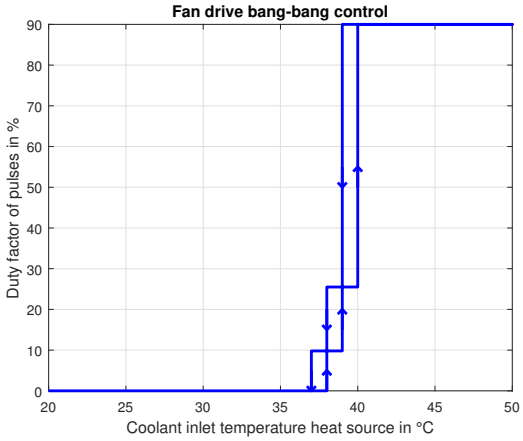

Figure 6.4: Bang-bang control

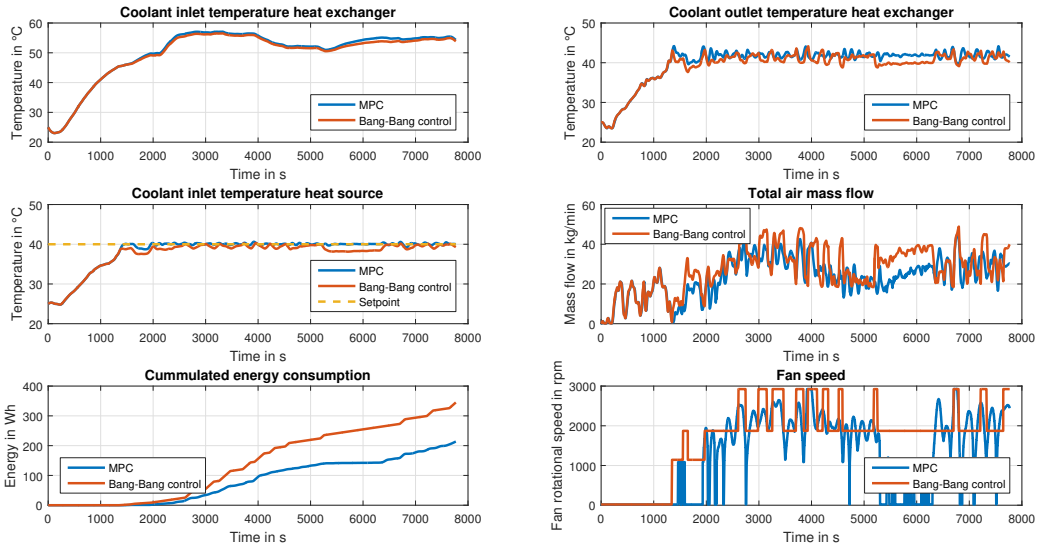

Figure 6.5: Comparison between bang-bang control and MPC

6.3 Outlook and Limitations

For further investigations a new, smaller test bench would present a significant improvement, as the current one contains over $80kg$ of coolant mass. In relation to the large coolant mass the coolant mass flow of $\dot{m}_{co} = 8\frac{kg}{min}$ is much to small. In addition there are several unknown masses, like junctions or the conditioning unit's coating. Additionally, it is not possible to simulate the air mass flow caused by a moving vehicle at the test bench or implement a second MPC to control the speed of the cooling pump.
Another task would be to prove the stability of the Constrained Model Predictive Control and the PI observer. Furthermore, the MPC was implemented with fixed constraints. For example, the maximum cooling capacity in the control algorithm was set as a constant parameter, although it depends on several parameters like coolant mass flow, coolant and air temperature. Also, the energy saving may be improved further by implementing a different cost function for the Model Predictive Control.

Bibliography

[1] Rawlings James Blake and Mayne David Q. *Model Predictive Control : Theory and Design*. 5th. Madison, Wis. Nob Hill Pub. cop., 2015. ISBN: 9780975937709 (cit. on p. 32).

[2] S. S. Butt, R. Prabel, and H. Aschemann. "Robust input-output linearization with input constraints for an engine cooling system." In: *2014 American Control Conference*. 2014, pp. 4555–4560. ISBN: 0743-1619. DOI: 10.1109/ACC.2014.6858647 (cit. on pp. 1, 2).

[3] Cengel. *Heat Transfer a Practical Approach Si Ve*. Englisch. 3rd. New Delhi etc.: Mcgraw Hill Higher Education, 2006. ISBN: 9780070634534 (cit. on pp. 17, 18).

[4] Yu-Juei Chang and Chi-Chuan Wang. "A generalized heat transfer correlation for louver fin geometry." In: *International Journal for Heat and Mass Transfer* 40.3 (3 1997), pp. 533–544. DOI: 10.1016/0017-9310(96)00116-0. URL: http://dx.doi.org/10.1016/0017-9310(96)00116-0 (cit. on p. 18).

[5] D.A. D'Esopo. "A convex programming procedure." In: *Naval Research Logistics Quarterly* 6.1 (Mar. 1959), pp. 33–42. DOI: 10.1002/nav.3800060105 (cit. on p. 40).

[6] C.G. Hildreth. "A quadratic programming procedure." In: *Naval Research Logistics Quarterly* 4.1 (Mar. 1957), pp. 79–85. DOI: 10.1002/nav.3800040113 (cit. on p. 40).

[7] Martin Horn and Nicolaos Dourdoumas. *Regelungstechnik*. Pearson Deutschland, 2003. ISBN: 9783863265533 (cit. on p. 30).

[8] H.P. Künzi, W. Krelle, and R. von Randow. "Das Verfahren von Hildreth und d'Esopo." In: *Nichtlineare Programmierung*. 1979 (cit. on pp. 37, 41).

[9] D. Luenberger. "An introduction to observers." In: *IEEE Transactions on Automatic Control* 16.6 (Dec. 1971), pp. 596–602. DOI: 10.1109/TAC.1971.1099826 (cit. on p. 44).

[10] K. Narendra and P. Gallman. "An iterative method for the identification of nonlinear systems using a Hammerstein model." In: *IEEE Transactions on Automatic Control* 11.3 (July 1966), pp. 546–550. DOI: 10.1109/TAC.1966.1098387 (cit. on p. 27).

[11] Heinz Petutschnik. "Entwicklung einer Simulationsmethodik zur Abbildung des thermischen Management von Motor und Fahrzeug." Dissertation. Technische Universität Graz, 2007 (cit. on p. 4).

[12] Page R., Hnatczuk W., and J. Kozierowski. "Thermal Management for the 21st Century - Improved Thermal Control and Fuel Economy in an Army Medium Tactical Vehicle." In: *SAE Technical Paper 2005-01-2068* (2005). DOI: 10.4271/2005-01-2068 (cit. on p. 1).

[13] Dirk Söffker, Tie-Jun Yu, and Peter C. Müller. "State estimation of dynamical systems with nonlinearities by using proportional-integral observer." In: *International Journal of Systems Science* 26.9 (Sept. 1995), pp. 1571–1582. DOI: 10.1080/00207729508929120 (cit. on p. 44).

[14] A. Traussnig, M. Stolz, and M. Horn. "MPC based Fan Control for Automotive Applications." In: *IFAC-PapersOnLine* 49.11 (2016). 8th IFAC Symposium on Advances in Automotive Control AAC 2016Norrköping, Sweden, 20—23 June 2016, pp. 399–405. ISSN: 2405-8963. DOI: http://dx.doi.org/10.1016/j.ifacol.2016.08.059. URL: http://www.sciencedirect.com/science/article/pii/S2405896316313994 (cit. on p. 5).

[15] Armin Traussnig and Michael Stolz. "Vehicle Thermal Management Simulation Method Integrated in the Development Process from Scratch to Prototype." In: *SAE 2014 World Congress & Exibition*. 2014. ISBN: 2014010668. DOI: 10.4271/2014-01-0668 (cit. on pp. 14, 15, 20, 22).

[16] VDI-Wärmeatlas. Ed. by VDI-Gesellschaft Verfahrenstechnik und Chemieingenieurwesen (GVC). 10th. Springer, Berlin, 2006. ISBN: 3540255044. DOI: 10.1007/978-3-540-32218-4 (cit. on pp. 13, 19).

[17] Liuping Wang. *Model Predictive Control System Design and Implementation Using Matlab*. Springer-Verlag London, 2009. ISBN: 9781848823310. DOI: 10.1007/978-1-84882-331-0 (cit. on pp. 37, 43).

[18] Zou X., Jordan J., and M. Shillor. "A dynamic model for a thermostat." In: *Journal of Engineering Mathematics* 36 (4 1999), pp. 291–310. DOI: 10.1023/A:1004587425961 (cit. on p. 2).